Aus dem Cécile und Oskar Vogt Institut für Hirnforschung

der Heinrich-Heine-Universität Düsseldorf

Direktorin: Univ. Prof. Dr. med. Katrin Amunts

Two new areas in the human frontal operculum: Cytoarchitecture, stereotaxic maps and brain function

Dissertation

zur Erlangung des Grades eines Doktors der Medizin

der medizinischen Fakultät der Heinrich-Heine-Universität Düsseldorf

vorgelegt von

Martin Saal

2019

Als Inauguraldissertation gedruckt mit Genehmigung der
Medizinischen Fakultät der Heinrich-Heine-Universität Düsseldorf

gez.: Martin Saal

Dekan: Univ.-Prof. Dr. med. Nikolaj Klöcker

Erstgutachterin: Univ.-Prof. Dr. med. Katrin Amunts

Zweitgutachter: Univ.-Prof. Dr. med. Simon B. Eickhoff

Gewidmet meinen Eltern und meiner Ehefrau, für Ihre unnachlässige und bedingungslose Unterstützung.

Summary

The present study identifies and provides an analysis of two new areas, OP8 and OP9, in the frontal operculum. For cortical mapping, a well-established observer-independent cytoarchitectonic mapping approach was used. Serial, cell body stained sections of ten post mortem brains were evaluated using light microscopy, image analysis and statistical tools to determine the areal cytoarchitectonic characteristics, their differences to adjacent areas and to identify their localisation in the cortical ribbon. Based on the resulting individual maps of OP8 and OP9 in each examined brain, probability maps were calculated, which provide measures of interindividual variability in stereotaxic MNI reference space.

OP8 and OP9 are located in the depth of the lateral fissure, laterally from the circular insular sulcus. Area OP8 is positioned more caudally than OP9. The “classical Broca’s areas” BA44 and BA45 are directly latero-dorsally adjoining for both areas. Furthermore areas OP6 and OP7 border OP8 in caudal direction, while area OP10 borders OP9, representing the rostrally neighbouring area in the frontal operculum. Both areas do not reach to the free lateral brain surface, but are located in the depths of the lateral fissure. Approximate anatomical landmarks are the inferior precentral sulcus as a caudal and the ascending branch of the lateral fissure as a rostral limitation for OP8, while OP9 reaches from the ascending branch of the lateral fissure to the rostral ending of the horizontal branch of the lateral fissure.

Applying these cytoarchitectonic results to functional studies especially constitutes language functions to OP8 and OP9. Due to their small volume and limitations in MRI resolution, a decided functional segregation was not possible yet. They were examined as part of a bunch of areas forming the frontal operculum.

The new cytoarchitectonic maps of areas OP8 and OP9 will serve as a basis for more detailed neuroimaging studies to decipher the specific functions of this circumscribed part of the frontal operculum as well as its functional connectivity, especially with respect to their role in the language networks. According to our meta-analysis this might verify the frontal operculum as component of an “extended Broca area”.

Zusammenfassung

Die vorliegende Studie beschreibt zwei neue Areale, OP8 und OP9, im frontalen Operculum. Die Grenzen wurden unter Verwendung eines etablierten, Untersucher-unabhängigen Verfahrens zur zytoarchitektonischen Kartierung identifiziert. Serielle, Zellkörper-gefärbte Schnitte von zehn post mortem Gehirnen wurden mittels Lichtmikroskopie, Bildanalyse und statistischer Verfahren analysiert, um die zytoarchitektonischen Charakteristika der Areale, ihre Unterschiede zu angrenzenden Arealen, sowie ihre Lage im Kortex zu bestimmen. Basierend auf den daraus resultierenden Karten von OP8 und OP9 in jedem der untersuchten Gehirne, wurden Wahrscheinlichkeits-Karten berechnet, welche die interindividuelle Variabilität im stereotaxischen MNI-Raum quantifizieren.

OP8 und OP9 befinden sich in der Tiefe der lateralen Fissur, lateral des zirkulären insulären Sulcus. Area OP8 ist weiter kaudal als OP9 gelegen. Die „klassischen Broca-Areale“ BA44 und BA45 grenzen direkt latero-dorsal an beide Areale an. OP6 und OP7 grenzen von kaudal an OP8, während OP9 rostral an OP8 anschließt. Die rostrale Begrenzung von OP9 wiederum wird vom bisher noch nicht näher kartierten Areal OP10 gebildet. Sowohl OP8, als auch OP9, erreichen nicht die freie laterale Hirnoberfläche, sondern befinden sich in der Tiefe der lateralen Fissur. Ungefähre makroanatomische Landmarken sind der inferiore Anteil des Sulcus praecentralis als kaudale und der Ramus ascendens der Fissura lateralis als rostrale Grenze für OP8, während OP9 vom Ramus ascendens der Fissura lateralis bis zum rostralen Ende des Ramus horizontalis der Fissura lateralis reicht.

Wendet man diese zytoarchitektonischen Ergebnisse auf funktionelle Studien an, ergeben sich für OP8 und OP9 insbesondere Sprachfunktionen. Aufgrund ihres kleinen Volumens und der limitierten Auflösung von Magnetresonanztomographien, war eine dezidierte funktionelle Auftrennung bislang nicht möglich. Sie wurden daher als Anteil mehrerer Areale untersucht, welche insgesamt das frontale Operculum bilden.

Die neuen zytoarchitektonischen Karten der Areale OP8 und OP9 können als Grundlage für neue bildgebende Studien dienen, um die spezifischen Funktionen dieser neuen Areale im frontalen Operculum zu entschlüsseln, ebenso wie deren funktionelle Verbindungen, vor allem hinsichtlich ihrer Rolle in sprachverarbeitenden Netzwerken. Entsprechend unserer Meta-Analyse könnte dies die Annahme, dass das frontale Operculum unter anderem Teil eines „erweiterten Broca Areals“ ist, bekräftigen.

Abbreviations

aIf	ascending branch of the lateral fissure	**aI**	anterior insula
ALE	activation likelihood estimation	**BA**	Brodmann area
BD	behavioural domain	**BDPC**	behavioural domains and paradigm classes
cis	circular insular sulcus	**cs**	central sulcus
dIII/dV	deep part of lamina III / V	**dACC**	dorsal anterior cingulate cortex
ds	diagonal sulcus	**ED**	Euclidean distance
EEG	electroencephalography	**ELAN**	early left anterior negativity
ERP	event-related potentials	**F*Bop***	Area frontalis agranularis in operculo
F*CDop*	Area frontalis intermedio granularis in operculo	**F*Dop***	Area frontalis granularis in operculo
FDR	false discovery rate	**Fig.**	Figure
F*F*	Area orbitalis	**fMRI**	functional magnetic resonance imaging
FOP	frontal operculum	**FSG**	finite state grammar
GLI	grey level index	**hlf**	horizontal branch of the lateral fissure
Iad7	anterior dorsal insula	**IC**	insular cortex
ifs	inferior frontal sulcus	**IFG**	inferior frontal gyrus
lf	lateral fissure	**mIII/mV**	mid part of lamina III / V
MACM	meta-analytic connectivity modelling	**MEG**	magnetencephalography
MNI	Montreal Neurological Institute	**MPM**	maximum probability map

MRI	magnetic resonance imaging
OP	area opercularis
prs	precentral sulcus
PNFA	progressive nonfluent aphasia
ROI	region of interest
SD	standard deviation
ts	triangular sulcus
wm	white matter
msFC	medial superior frontal cortex
PC	paradigm class
PET-CT	positron emission tomography - computer tomography
PSG	phrase structure grammar
SII	secondary somatosensory cortex
STG	superior temporal gyrus
uIII/uV	upper part of lamina III / V

Table of contents

Introduction 1
Material and Methods 4
Brain preparation 4
Digital observer-independent border detection 5
Calculation of areal volumes 8
Hierarchical cluster analysis 9
3D reconstruction and probability maps 10
Functional and connectivity analytics 10
Behavioral Domains and Paradigm Classes (BDPC) 11
Meta-analytic connectivity modelling (MACM) 12
Results 13
Cytoarchitectonic description of OP8 and OP9 13
Correlation with anatomical landmarks and neighbouring areas 29
Volumes of OP8 and OP9 30
Cytoarchitectonic dependency by hierarchical cluster analysis 32
Probability in stereotaxic space 33
Functional attribution and co-activation analysis by meta-analytic connectivity modelling 37
Discussion 45
Comparison with brain maps of Brodmann and Economo & Koskinas 45
Integration of cytoarchitectonic delineation into functional imaging analysis 47
Connection of the FOP to other language related areas 47
The role of OP8 and OP9 in language processing 49
Lateralization of function of OP8 and OP9 52
Functional interareal differentiation of OP8 and OP9 52
Further evidence of lateralization of function beyond language processing 53
Pain dependent activation of the FOP 54
Diseases effecting the FOP besides direct lesions 55
Conclusion 56
References 58

Introduction

Korbinian Brodmann has established a brain map describing the segregation of the cerebral cortex based on cytoarchitecture, i.e. on regional differences in the shape, size and arrangement of cell bodies (Brodmann, 1909). This map became one of the most cited reference for cortical areas (for an overview, see Amunts and Zilles, 2015). It represents the view of a lateral surface of a single human brain hemisphere, and does not provide details about borders between areas within the sulci including the frontal operculum. Though about 60% of the cerebral cortex are not on the free surface, but are located in the depths of the sulci (Zilles et al., 1988). Later in the 20th century, von Economo & Koskinas realized that an areal classification solely based on descriptive aspects is exposed to subjective criteria as well as experience and anticipation – they therefore introduced quantitative indicators of cortical areas including measures of cortical thickness, layer thickness or cell size, which also included the depths of sulci (Economo and Koskinas, 1925).

Several brain maps using different methods of investigation with a differing number of brain areas and classification schemes have been published, despite the relatively young history of brain mapping (Bailey and Bonin, 1951; Campbell and Schlesinger, 1905; Economo and Koskinas, 1925; Flechsig, 1920; Sarkisov et al., 1949; Vogt and Vogt, 1919), some of them specialising on a certain brain region (Ongür et al., 2003; Sanides, 1962). Brodmann as well as Economo & Koskinas mentioned that, in addition to sharp, doubtlessly well distinguishable inter-areal borders, there are also complex transitions between areas. For example, differences between areas may evolve in the different laminae at slightly different positions of the cortical ribbon (Amunts et al., 1999; Amunts et al., 2000; Bludau et al., 2014; Caspers et al., 2006; Choi et al., 2006; Eickhoff, Schleicher et al., 2006; Geyer et al., 1999; Henssen et al., 2016). Furthermore, macroanatomical features of the brain do not always co-vary with the cytoarchitecture and inter-individual differences have been reported for both aspects of brain organisation (Amunts and Zilles, 2015; Duvernoy and Bourgouin, 1999; Economo and Koskinas, 1925; Ono et al., 1990; Petrides and Pandya, 2012; Roland et al., 1997; Zilles and Amunts, 2013).

In order to reliably identify and analyse cytoarchitectonic areas, an observer-independent delineation of brain areas is mandatory, which in this study is based on the statistical determination of borders by maximum differences in feature vectors of the cytoarchitecture of individual areas in a representative sample of post-mortem brains (Schleicher et al., 1999).

This approach was applied, for example, in the parietal operculum (Eickhoff, Schleicher et al., 2006). It identified, for the first time, four unique areas located in the depths of the lateral fissure (areas OP1-4). This new subdivision was subsequently correlated with results from functional magnetic resonance imaging (fMRI) studies of the secondary somatosensory cortex (SII) to elucidate the functional role of these areas (Eickhoff, Amunts et al., 2006).

The new parcellation of the parietal operculum raised the question of whether there are additional, unknown areas located more rostral to the parietal operculum, in the frontal operculum. This hypothesis was supported by evidence coming from a study of our lab investigating the molecular architecture of the frontal operculum by analysing the receptor architecture of neurotransmitter of Broca's region and surrounding cortices (Amunts et al., 2010). That study proposed a first cytoarchitectonic footprint of two new areas, OP8 and OP9, and described their receptor architecture and localisation.

In addition, there are several studies reporting different activation patterns in the frontal operculum by fMRI and other in vivo imaging methods. Due to the spatial resolution of fMRI studies, many of such studies refer to the frontal operculum (FOP) as a whole, but do not distinguish between the specific involvement of separate areas. OP8 and OP9 seem to be part of the FOP and thus inter alia integrated in language processing (Anwander et al., 2007; Friederici, Fiebach et al., 2006; Riès et al., 2013; Stromswold et al., 1996). The FOP could be seen as a part of a "functionally extended Broca's area" together with the obligatory BA44 and BA45, as well as BA47 and the ventral premotor cortex (Hagoort, 2005).

The FOP – together with the left anterior superior temporal gyrus (STG) (Friederici, 2002; Meyer, E. et al., 2000) and the left putamen (Friederici et al., 2003) - showed to be responsible for on-line syntactic structure building

(Rolston et al., 2015) and speech processing (Friederici et al., 2000). Contrariwise neighbouring BA44 and BA45 as well as BA47 are involved in more complex syntactic processing (Dapretto and Bookheimer, 1999; Just et al., 1994; Rolston et al.; Stromswold et al., 1996). The connection to the basal ganglia may be key in explaining the FOP as part of a procedural memory circuit for syntactic processing (Stromswold et al., 1996; Ullman et al., 1997; Ullman, 2001). Regarding lateralization, the right FOP seems to be more activated by auditory stimulus than sentence reading, as well as the processing of prosody / intonation (Friederici et al., 2000, pp. 297–298; Meyer, M. et al., 2000). By meta-analysis using activation likelihood estimation (ALE) based meta-analytic connectivity modelling (MACM) (Eickhoff et al., 2010; Laird et al., 2005; Turkeltaub et al., 2002) based on the maximum probability maps now established, we will link the results of previous functional studies with possible areal connections and functional networks.

Thus, based on these findings from neuroimaging and our own study regarding the molecular architecture of the FOP, the present study aims to define the cytoarchitectonic characteristics of OP8 and OP9 in a comprehensive manner, and to determine their borders based on cytoarchitectonic, yet observer-independent methods. Such approach results in probabilistic 3D maps and is then used as a tool to correlate the cytoarchitectonic segregation with functional, fMRI-based data to analyse the functional relevance of areas OP8 and OP9 and their role in different neuronal networks using MACM.

Material and Methods

Brain preparation

We analysed histological sections of 10 post mortem brains from body donors of the Anatomical Institute of the University of Düsseldorf. The body donors gave written informed consent. The study was approved by the local ethics committee. The brains were removed from the scull after a maximum of 24 hours post mortem. There were no relevant pre-existing neurological or psychiatric diseases (brain number 3 and 9 with documented small cerebral infarction, but not in the region of interest) (see **Table 1**).

brain code	age (years)	sex	medical history
1	79	w	bladder carcinoma
2	56	m	rectum carcinoma
3	69	m	vertebrobasilar aneurysm, multiple cerebral infarctions
4	75	m	rapidly progressive glomerulonephritis
5	59	w	cardiorespiratory insufficiency
6	54	m	coronary heart disease, myocardial infarction, colitis ulcerosa
7	37	m	acute right heart failure, hepatic coma
8	72	w	renal failure
9	79	w	atherosclerosis, aortic stenosis, left heart insufficiency, basal ganglia infarction
10	85	w	small bowel obstruction, mesenterical infarction

Table 1: Post mortem brains and their characteristics used for cytoarchitectonic analysis
Median age 66,5 years. Equal distribution between sexes. Handedness unknown (right handed subjects 90% incidence in population (Annett 1973). Language dominance unknown. All cutting planes coronal. *w*, female; *m*, male

The brains were fixed for at least 6 months using 4% formalin or Bodian's solution, hanging up on the arteria basilaris or vertebralis to avoid deformation. After fixation the brains were scanned by MRT (1.5 Tesla Siemens Magnetom SP Scanner, 3D FLASH pulse sequence, flip angle 40°, repetition time 40 ms, echo time 5 ms, voxel size 1.17x1x1 mm). After gradual dehydration by ethanol, repeated washing in chloroform and embedment in paraffin, they were cut in coronal plane using a microtome (Polycut E, Reichert-Jung, Deutschland) resulting in a thickness of 20 µm per section. By that, up to 7600 slices per brain

were produced according to the different brain sizes. For microscopical analysis each 15th section was stained with a modified silver staining (Merker, 1983; Uylings et al., 1999) of the perikaryon, resulting in darkly stained cell bodies in cortex and white matter. For the final mapping, each 60th section of the total number (i.e. each 4th stained section) was used, resulting in a distance of 1.2 mm between sections. Where damage or artefacts due to the prior preparation procedure or unfavourable course of the cortex made investigation impossible or uncertain, the nearest suitable stained section was used. The whole procedure has been described elaborately in the past (Amunts et al., 1999). The sections were scanned by a flatbed scanner in 1200 dpi 8-bit grey scale resolution, resulting in 20 µm/pixel. This was important for the following digital 3D reconstruction, as comparing to the MRI scan of the intact brain allowed mathematical compensation of procedure inherent bias like shrinking (Amunts et al., 2004; Henn et al., 1997; Mohlberg et al., 2003).

Digital observer-independent border detection

The examination of cytoarchitectonic cortical borders was based on the grey level index (GLI) for observer-independent, objectively reproducible results (Amunts and Zilles, 2001; Schleicher et al., 1999; Schleicher et al., 2005; Schleicher et al., 2009; Zilles, Schleicher et al., 2002). The region of interest (ROI) was defined as a rectangular area containing the rostral part of the lateral fissure (lf) forming the ventral limit of BA44 and BA45. The ROI were marked on every examined section and scanned by a CCD camera (Axiocam MRm, ZEISS, Germany) mounted on a light-optical microscope (Axioplan 2 Imaging, ZEISS, Germany; 10x magnification). The sections were moved in a meander like pattern by a motor controlled microscope stage. Camera and stage were controlled by an image analysing software (KS400, version 3.0, ZEISS, Germany; Axiovision, version 4.6, ZEISS, Germany). The digitization was carried out with a solution of 1.02 µm/pixel. The digital scans were then processed into GLI images by using above mentioned image analysing software (Schleicher and Zilles, 1990) and an in-house written tool for MatLab (The Mathworks, Inc., Natick MA). Then two Gaussian filters (radius 1 pixel and 40 pixels) were applied and both images substracted from each other to carve out

the silhouette of the cell bodies. Applying a threshold preceded to a binary image, which was overlaid by a grid of 16x16 pixels. The 8-bit grey values of a GLI image coded for the volume fraction of cell bodies in a square of these 16x16 pixels in the original ROI and thereby reflected cytoarchitectural properties (Wree et al., 1982). More white pixels encoded for cells, while more dark pixels encoded neuropil redundant for further examination of the cortical layers. These images were later inverted, to be similar to the distribution of grey levels in histological sections.

The MatLab software tool was also used for the following steps. The inner (lamina VI – white matter) and outer (lamina I – lamina II) borders of the cortex were marked by contour lines that built the internal frontier for curvilinear traverses following the principles of electric field lines (Jones et al., 2000). The GLI values inherent of the traverses formed profiles that were reviewed for ten features (mean GLI value, centre of gravity in x-direction, standard deviation, skewness, kurtosis, as well as the corresponding first derivate) (Dixon, 1988; Schleicher et al., 1999; Schleicher and Zilles, 1990). To avoid bias by differing cortical thickness, the profiles were standardised by linear interpolation to a standard thickness of 100% formed by the lamina VI – white matter border. For multivariate distance analysis we used the Mahalanobis distance (Mahalanobis et al., 1949) as a measurement representing the degree of difference between the cytoarchitecture of profiles. The Mahalanobis distance was calculated between the ten features of adjacent profiles by using a sliding window procedure (Schleicher et al., 1999; Schleicher and Zilles, 1990) encircling every profile and with blocks consisting of a defined amount of adjacent profiles (10 to 24 profiles per block). The higher the Mahalanobis distance, the higher the differences of the feature vectors of the compared profiles. Using Hotelling's T2-Test with Bonferroni correction unmasked borders located exactly on the centre of the blocks by providing significant maxima of the distance function of the different block sizes (Schleicher et al., 1999). It is thereby observer-independent. The resulting borders were verified by light microscopy. This was necessary, as e.g. tangential cuts of inner-cortex vessels or cutting or staining artefacts resulted in an automated border detection and needed to be excluded. For a graphic overview of the main steps of observer-independent border

detection, see **Figure 1**. Thus, individual maps highlighting the extent of OP8 and OP9 in each hemisphere in each of the ten examined brains could be processed (see **Figure 2**).

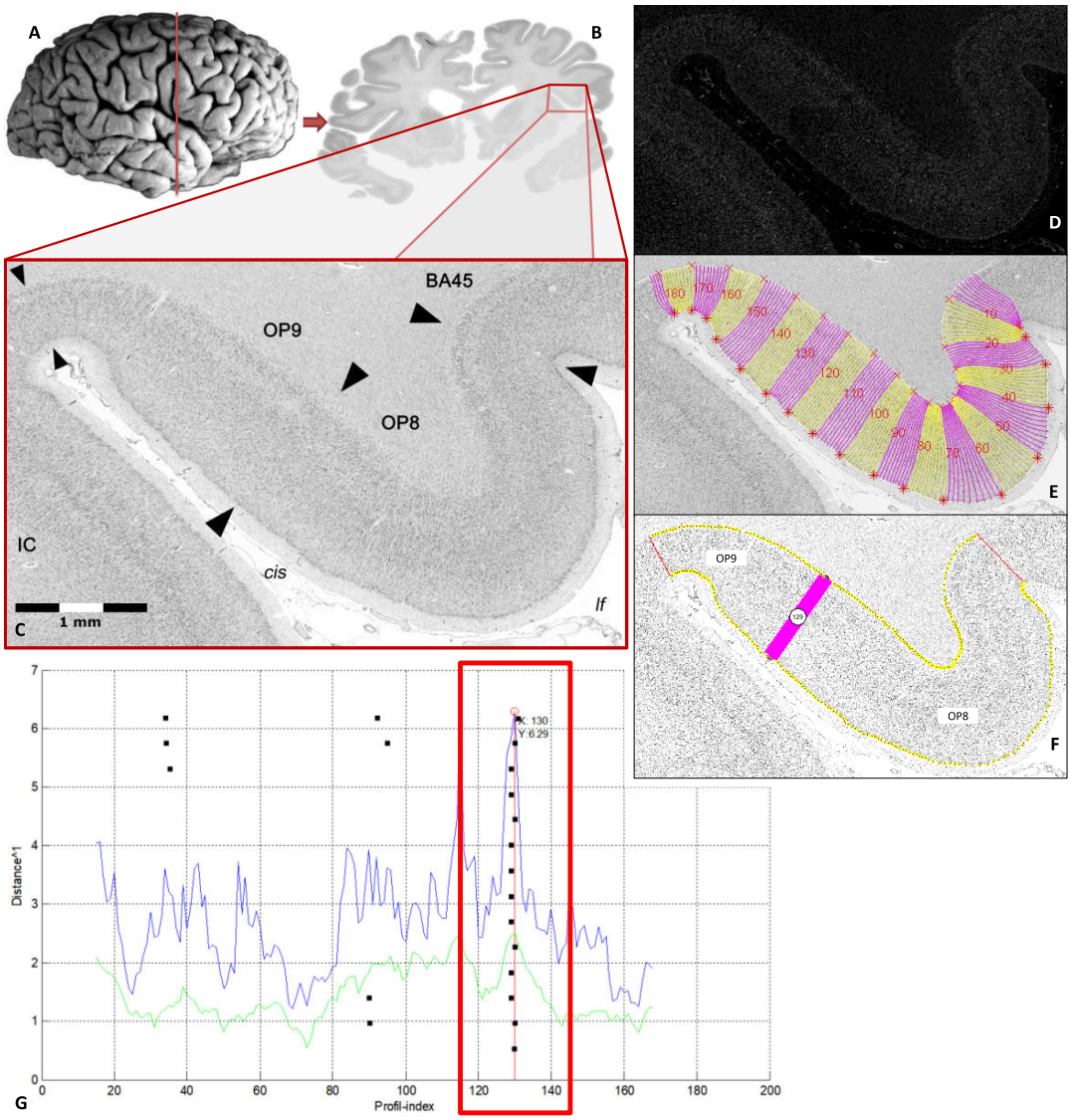

Fig. 1: Cytoarchitectonic border detection between OP8 and OP9

(A) Right lateral brain view, red line marks cutting plane of the corresponding coronal section **(B)**. **(C)** Microscopical scan with borders (arrow heads) of OP8, OP9 and adjacent BA45 and insular cortex (IC). Each third of the scale in the lower left corner measures 1 millimeter in the original scan. *If,* lateral fissure; *cis,* circular insular sulcus. **(D)** GLI-image of the scan. **(E)** Parcellation of the cortex in equidistant profiles. **(F)** Observer-independent border detection at profile 129 with corresponding distance function (here for block size 15) and dot blot marking the most probable border position (**G**).

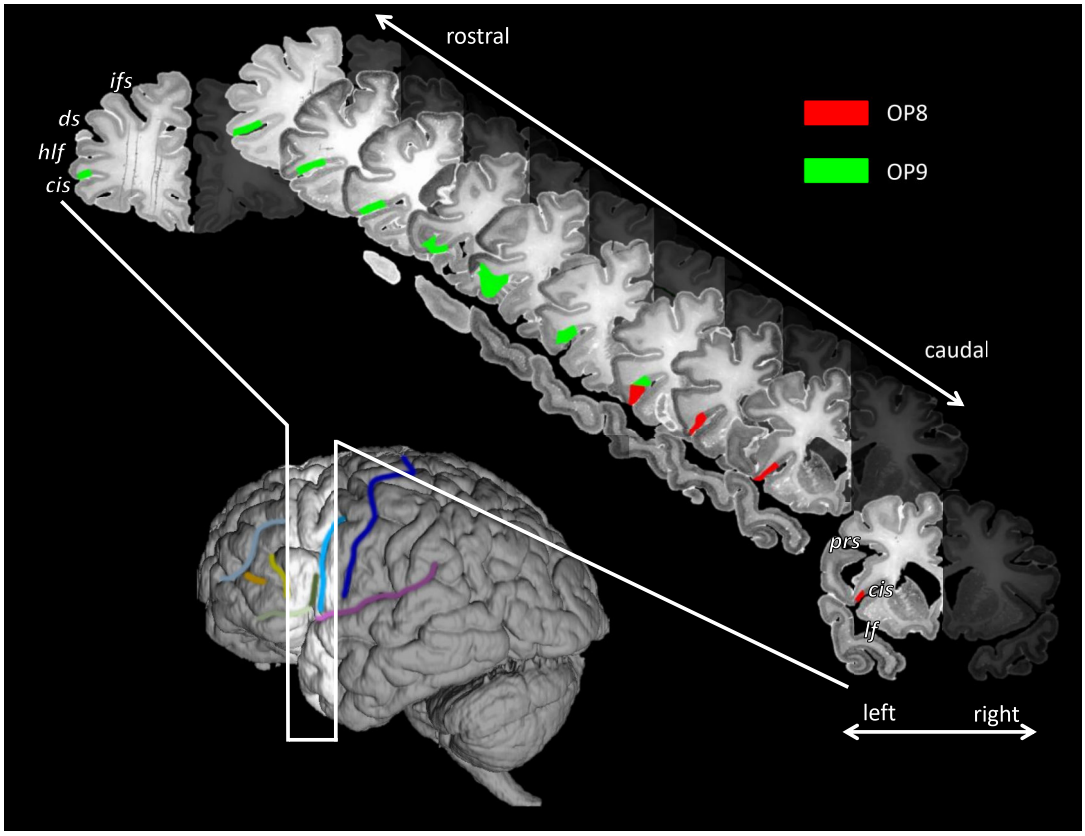

Fig. 2: Individual evolution of the areas OP8 and OP9 marked on sections in brain 09 in rostrocaudal direction

Most rostral and most caudal section shifted for better visualisation of the sulci. Right hemisphere and brain areas not represented in the sections are greyed out. Areal location in the sections is marked by colours: OP8 red, OP9 green. The lower left corner shows a reconstruction of the scanned sections of the whole brain from a left lateral view, the white lines mark the most rostral and most caudal section. Colours mark the different sulci: central sulcus (dark blue), precentral sulcus / *prs* (cyan), inferior frontal sulcus / *ifs* (light blue), lateral fissure / *lf* (purple), ascending branch of the lateral fissure (dark green), horizontal branch of the lateral fissure / *hlf* (light green), diagonal sulcus / *ds* (yellow), triangular sulcus (orange); circular insular sulcus / *cis* not visible from a lateral superficial view.

Calculation of areal volumes

Estimation of areal volumes of OP8 and OP9 was done based on delineations of areas in the digitized sections. The Cavalieri principle (Howard and Reed, 1998; Uylings et al., 1986; Uylings et al., 1999) was applied based on the formula "$V = s \cdot T \cdot x \cdot y \cdot \Sigma A_i \cdot F$" measuring the volume "V" in mm³. "s" is the number of sections between two measuring points (usually 60), "T" is the thickness of each section (20 µm), "*x*" and "*y*" are the width and height of a pixel

in the digitized section (21.16 µm), "ΣAi" is the sum of all pixels of the specific area. "F" is the shrinkage factor of the particular brain for shrinkage corrected true volume measurement (Amunts et al., 2005). These volumes were then normalized by building a quotient of the whole brain volume and the corrected volume. Otherwise, bias would occur due to e.g. the physiologically bigger brain volume in male humans.

By using a non-parametric pair-wise permutation test (Bludau et al., 2014), the areas were compared regarding inter-hemispheric and sex differences.

Hierarchical cluster analysis

For each area OP8 and OP9, as well as adjacent BA44, BA45 and BA47, sample regions consisting of 15 GLI profiles were extracted from 3 different sections from each hemisphere of each brain, thus resulting in distinct mean GLI profiles. These profiles were chosen by cytoarchitectonic criteria, i.e. preferably containing no blood vessels, no artefacts from cutting or staining and of perpendicular orientation to the cortex. Mean feature vectors were extracted from the mean GLI profiles (analogue to the extraction of feature vectors for border detection) of each area per hemisphere and further processed by calculating the Euclidean distance (ED) and applying the Ward linking method (Ward jr., 1963). While aforementioned extraction of feature vectors for border detection was based on the Mahalanobis Distance, which accounts for individual differences between the areas, we here used the Euclidean distance as it is independent of intraareal variance (Schleicher et al., 2000; Schleicher et al., 2005). This procedure resulted in a hierarchical clustering analysis and thereby a further observer-independent comparison of OP8 and OP9 with their adjacent areas. It allowed regrouping the areas according to their degree of cytoarchitectonic similarity and dissimilarity and illustrate this in form of a dendrogram. The higher the ED and thus the higher the cytoarchitectonic dissimilarity between areas, the larger the distance between them in the dendrogram and vice versa for similarity.

3D reconstruction and probability maps

The areal borders were traced in the high resolution scans mentioned above using in-house software tools. 3D reconstruction was then performed via the initial individual MRIs of the fixed brains (Amunts et al., 2000; Hömke, 2006). Afterwards, OP8 and OP9 of all investigated brains were transferred to the anatomical reference space of the T1-weighted MRI of the single subject template of the Montreal Neurological Institute (MNI) (Evans et al., 1992; Evans et al., 1994; Evans et al., 2012) via linear affine and nonlinear elastic transformation (Evans et al., 1992; Henn et al., 1997; Hömke, 2006). Due to the MNI space slightly shifted out of the reference plain built by the anterior and posterior commissure (AC-PC plane), alignment was achieved by linear transformation of the anterior commissure as the reference structure 4 mm caudally and 5 mm dorsally, thus transferring into the so called “anatomical MNI space” (Amunts et al., 2005).

The individual maps of the areas were overlapped. Probability maps were calculated, which quantified the probability of finding an area at a certain stereotaxic coordinate. From these probability maps, a maximum probability map (MPM) (Eickhoff et al., 2005; Eickhoff, Heim et al., 2006) was calculated. Herein, each voxel represents the cortical area found in that exact position with maximum likelihood.

The centres of gravity of areas OP8 and OP9 in the maximum probability map were calculated for both hemispheres. These were located in the MNI space as described above. As most functional studies reported the centres of gravity of observed activation in the Talairach and Tournoux space, the coordinates were transformed using a MatLab tool (Brett, 2009, available at http://imaging.mrc-cbu.cam.ac.uk/ imaging/MniTalairach).

Functional and connectivity analytics

After defining the position of OP8 and OP9 in the MNI reference space, a meta-analytic connectivity modelling (MACM) was performed using modified activation likelihood estimation (ALE) (Eickhoff et al., 2009; Eickhoff et al., 2012; Laird et al., 2005; Turkeltaub et al., 2002) for each voxel to get a clue of their

possible functions as well as functional connections. This procedure used the BrainMap database (www.brainmap.org, Fox and Lancaster, 2002), which stored about 15,500 neuroimaging experiments at the time of demand, and describes the co-activation of foci in conjunction with OP8 and OP9. The fundament for the co-activation based analysis were the MPM used as seed regions. The search was made explicit on coordinates activated within at least one seed region. Thereby any nomenclature bias by differing naming of areas in the experiments could be eliminated, as only the coordinates in the Talairach and Tournoux reference space (Talairach et al., 1997) were used. To avoid bias of the co-activation data, the selection of studies was restricted in terms of healthy subjects. Studies investigating individual items (age, sex, handedness, etc.) were unaccounted for. In addition, only studies using fMRI and PET, as well as group analysis with at least 8 subjects were used. Our search revealed noticeably more experiments in the respective left hemisphere than for the right hemisphere. The number of experiments in detail was: OP8 left 455, OP8 right 299, OP8 total 651, OP9 left 471, OP9 right 315, OP9 total 713. The sum of an area's separate number of experiments does not match the total count, as there were experiments investigating activation combined in both hemispheric parts of the specific region.

Behavioral Domains and Paradigm Classes (BDPC)

For each of the experiments the meta-data "Behavioral Domains" (BD) and "Paradigm Classes" (PC) was stored (Laird et al., 2005). Behavioral Domains are defined as mental operations (action, cognition, emotion, interoception, perception) and their subcategories, e.g. action.preparation, cognition.language, emotion.anxiety, interoception.hunger, perception.somesthesis.pain (for all behavioral items, see http://www.brainmap.org/taxonomy/behaviors.html) (Fox et al., 2005). Paradigm Classes are the experimental tasks in each particular experiment, e.g. drawing, reading, tasting, writing (for all experimental items, see http://www.brainmap.org/taxonomy/paradigms.html). The frequency of all BPDC in OP8 and OP9 was compared to their appearance in the whole database, significantly frequent occurrence determined possible functions of the areas (Eickhoff et al., 2010). Significance of the local occurrence of a certain

domain or class was tested by χ^2 test (significance at $p < 0.05$). If significance was reached, the over- or under-representation of that domain or class was assessed by a binomial test (significance at $p < 0.05$). This test was repeated for the specific subdivisions of a domain or class. There was done forward as well as reverse characterization. The forward analysis tests whether a given task produces activation in the seed region more likely than activation per se. Reverse analysis tests whether activation in the seed region produces the task – behavioural domain or paradigm class – in question.

Meta-analytic connectivity modelling (MACM)

Possible functional connectivity was analysed by meta-analytic connectivity modelling (MACM) (Eickhoff et al., 2010; Laird et al., 2009). Each seed-voxel was tested for its connectivity with all other voxels of the brain. The BrainMap database was filtered for experiments that described activation in the above gathered stereotaxic coordinates of OP8 and OP9. These were then tested for consentaneous activation between each other by comparing their ALE scores to a null-distribution reflecting the random spatial uncertainty of each focus. Ergo the voxels within the seed region itself showed highest accordance, while accordance above chance in other brain regions suggested significant co-activation. Statistical certainty in terms of avoiding coincidental accumulation was achieved by testing these results against a null-distribution (Eickhoff et al., 2009; Eickhoff et al., 2012). Additionally, the results were corrected for multiple comparisons by applying the false discovery rate (FDR) (Laird et al., 2005).

Results

Two new areas based on an independent cytoarchitectonic mapping approach were defined, OP8 and OP9 in accordance to the previous identification based on receptor architectonic mapping (Amunts et al., 2010). Areas OP8 and OP9 were located in the depth of the frontal part of the lateral fissure (*lf*), ventrally neighbouring delineated areas BA44 at the opercular part and BA45 at the triangular part of the inferior frontal gyrus (Amunts et al., 1999; Amunts et al., 2010).

Cytoarchitectonic description of OP8 and OP9

Area OP8 has a dense but narrow lamina II, which presents as a dark stripe in the cortical ribbon. The transition of lamina II to III is sharp. Upper and mid lamina III are less dense than deep III with small to medium large pyramidal cells. In contrast, deep III has medium large prominent pyramidal cells. Lamina IV is narrow and thus sparse of granular cells, but still well visible and distinguishable as a ribbon separating lamina III and V. This characterizes OP8 as a dysgranular area. The infragranular lamina V has slightly prominent pyramidal cells in its upper subregion, while mid and deep V are less dense packed and thus appear more bright. Lamina VI again is more dense than lamina V, which enhances the contrast of a bright stripe of mid and deep V surrounded by darker upper lamina V and lamina VI. The transition of lamina VI to the white matter is mostly sharp. Only slight lamination (a distinguishable horizontal arrangement of cells within the laminae and thus producing the optical effect of building diffuse sublaminae) and slight visibility of columns (a distinguishable vertical arrangement of cells within the laminae und thus producing the optical effect of building columns/pillars; Buxhoeveden et al., 2000) can be seen.

Area OP9 also has a dense layer II and a sharp transition of lamina II to III. Upper and mid lamina III are far brighter due to less dense cell packaging. Alike OP8, deep lamina III has medium large prominent pyramidal cells. These seem more dominant than in OP8 because of the less dense upper and mid lamina III.

Lamina IV is a little bit more sparsely on granular cells than OP8 and narrow and only difficult to define, thus also classifying OP9 as dysgranular. Lamina V has only few prominent pyramidal cells in its upper subregion. Mid and deep lamina V consist of mostly granular cells and are similarly brightly packed as upper and mid lamina III, thus resulting in a bright ribbon under the deep section built by deep III and IV. Lamina VI consists of numerous small granular and pyramidal cells. The transition to the white matter is rather blurred. No distinct lamination or visibility of columns can be discriminated.

Both OP8 and OP9 are dysgranular areas, i.e. lamina IV is visible, but not that prominent as in granular BA45. Lamina IV is better visible in OP8 than in OP9, appearing as a ribbon separating laminae III and V. The ratio of supragranular lamina III and infragranular layer V is in favour of lamina III in both areas – corresponding to their adjoining areas (Amunts et al., 1999; Amunts et al., 2010). They commonly show medium large prominent pyramidal cells in deep lamina III. They especially differ in a bright lamina VI in OP8 versus a quite dense packed lamina VI in OP9. Furthermore, the slight lamination and visibility of columns of OP8 can't be seen in OP9 where all transitions are more or less diffuse.

The main criteria for identifying OP8 vs. BA44 is a slightly more dense lamina III with smaller pyramidal cells in deep III, the dysgranular IV which is visible as a fine thin ribbon and a less dense lamina V and VI with a more sharp border to the white matter.

OP9 and BA45 can be distinguished by a slightly more dense lamina III with smaller pyramidal cells, dysgranular lamina IV, only rarely prominent pyramidal cells in upper lamina V and a more sharp border to the white matter.

For an overview and comparison of the cytoarchitectonic features of OP8, OP9 and their adjoining areas OP6, OP7, OP10, BA44, BA45 and the unmapped area laterally of OP9 adjacent in the sulcus, see **Table 2**.

	Lamina	OP8	OP9
II	**density**	narrow, slightly dark stripe - less than OP6/OP7/BA45 - similar to BA44 - more than OP9 - much more than insula	- less than OP8/BA44 - similar to OP10 - more than BA45/unmapped area laterally adjacent in the sulcus - much more than insula
	II=>III	sharp	sharp
III	**uIII/mIII density**	uIII & mIII less dense than dIII overall density - less than OP7/BA44/BA45 - similar to OP6 - more than OP9/insula	consistent density - less than OP8/unmapped area laterally adjacent in the sulcus - more than OP10/BA44/BA45/ insula
	dIII	medium large prominent PC - smaller than OP7/BA44/BA45 - similar to OP6/OP9 - much more than insula	medium large prominent PC - less and smaller than BA44/BA45 - similar to OP8 - more prominent than OP10/ unmapped area laterally adjacent in the sulcus/insula
IV	**granularity**	dysgranular - less dense than OP6/OP7/BA44/ BA45 - similar to OP9 - much more dense than insula interstratified with small PC	dysgranular - similar to OP8/OP10 interstratified with small PC
	conspicuity	well visible ribbon - less than BA44/BA45 - similar to OP6/OP7 - more than OP9, much more than insula	moderately visible ribbon - less than OP8/OP10/BA44/ BA45 - similar to unmapped area laterally adjacent in the sulcus - much more than insula
V	**uV**	slightly prominent PC - less than OP6, much less than OP7 - similar to OP9/BA45 - more than BA44	slightly prominent PC - less than OP10/BA44/BA45 - similar to OP8/unmapped area laterally adjacent in the sulcus/insula

		slightly dark stripe	
	mV/dV	bright - less dense than OP6/OP7/BA44/ BA45 - similar to OP9 - more dense than insula	bright - less dense than BA44/BA45/ unmapped area laterally adjacent in the sulcus/insula - similar to OP8 - more dense than OP10
VI	**density**	bright - less dense than OP6/OP9 - similar to OP7/BA45 - more dense than BA44/insula	dense - less dense than BA44 - similar to BA45 - more dense but smaller cells than in OP8, more dense than OP10/unmapped area laterally adjacent in the sulcus/ insula
	VI=>wm	quite sharp - similar to OP7/BA45/insula - more sharp than OP6/OP9/BA44	blurred - less sharp than OP8 - similar to BA44/insula - more sharp than OP10/BA45
	Lamination	slightly - less than B44/BA45 - similar to OP6/OP7 - more than OP9/insula	almost not visible, mostly blurred transition of laminae - less than OP8/BA44/BA45/ insula - similar to OP10/unmapped area laterally adjacent in the sulcus
	Visibility of columns	slightly - less than OP7/BA44/BA45 - similar to OP6 - more than OP9/insula	almost not visible - less than OP8/BA44/BA45/ insula - similar to OP10/unmapped area laterally adjacent in the sulcus
	Visual contrast	II as dark ribbon, II-uV as noticeably dark ribbon	II & dIII & VI as noticeably dark ribbons

Table 2: Cytoarchitectonic features of OP8 and OP9 and their discrimination from particularly adjoining areas

The ratio of supragranular layers (III) to infragranular layers (V) is in favour of III in all areas. *PC*, pyramidal cells; *II=>III*, border between lamina II and III; *uIII / uV*, upper part of lamina *III / V; mIII / mV*, mid part of lamina III / V; *dIII / dV*, deep part of lamina *III / V*; *wm*, white matter; *VI=>wm*, border between lamina VI and white matter

For samples of the borders of the delineated areas with their neighbouring areas, see **Figures 3-13**. The microscopical scans were rotated where necessary and possible to standardize lamina I being the topmost lamina and the white matter being the lowermost subject. Areas BA44, BA45 and the yet uncharted area lateral of OP9 are located on the lateral brain surface, while areas OP6 till OP10 (not yet mapped) are located in the depth of the circular insular sulcus.

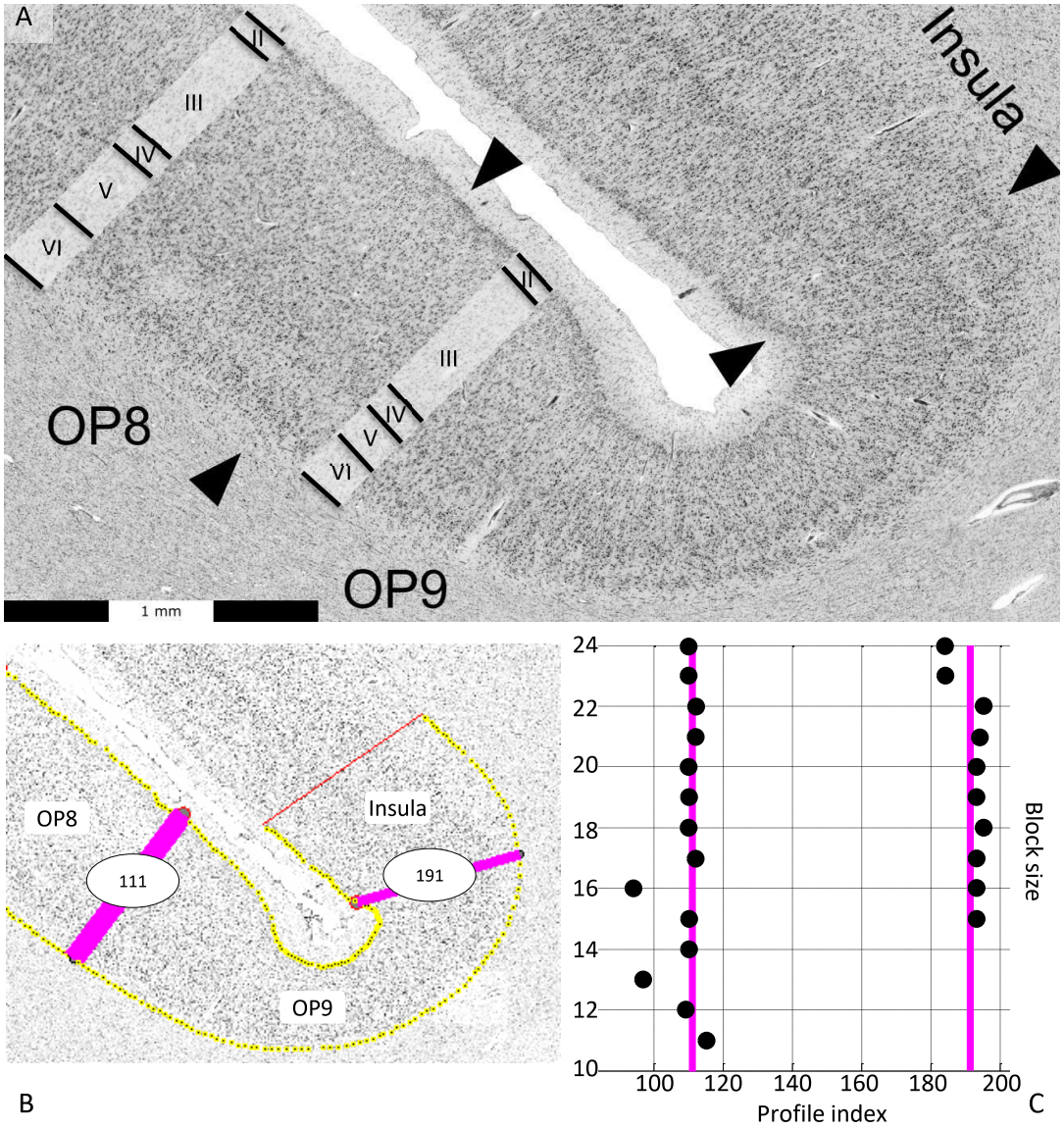

Fig. 3: Cytoarchitectonic border of OP8 and OP9 (A) with automatic border detection and dot blot illustrating the position of significant peaks (profile index) plotted against the block size

Roman numbers mark the laminae. Scale 1 mm per third. Notice that lamina II is less dense, and mid lamina III is more dense in OP8 than in OP9. Large pyramidal cells in both areas in deep III. Lamina IV is better visible in OP8, both areas are dysgranular. Lamina VI is brighter in OP8 while densly packed in OP9. Lamination and visibility of columns is more distinct in OP8. **(B)** Inverted GLI image after automatic border detection. Significant borders are shown as pink lines, together with the corresponding profile number, at which the border is found (profile 111 for border OP8 ⇔ OP9 and profile 191 for border OP9 ⇔ insula). **(C)** Dot blot with block sizes (ordinate) and profile index (abscissa). Dots indicate the profile index, at which the Mahalanobis distance was significant.

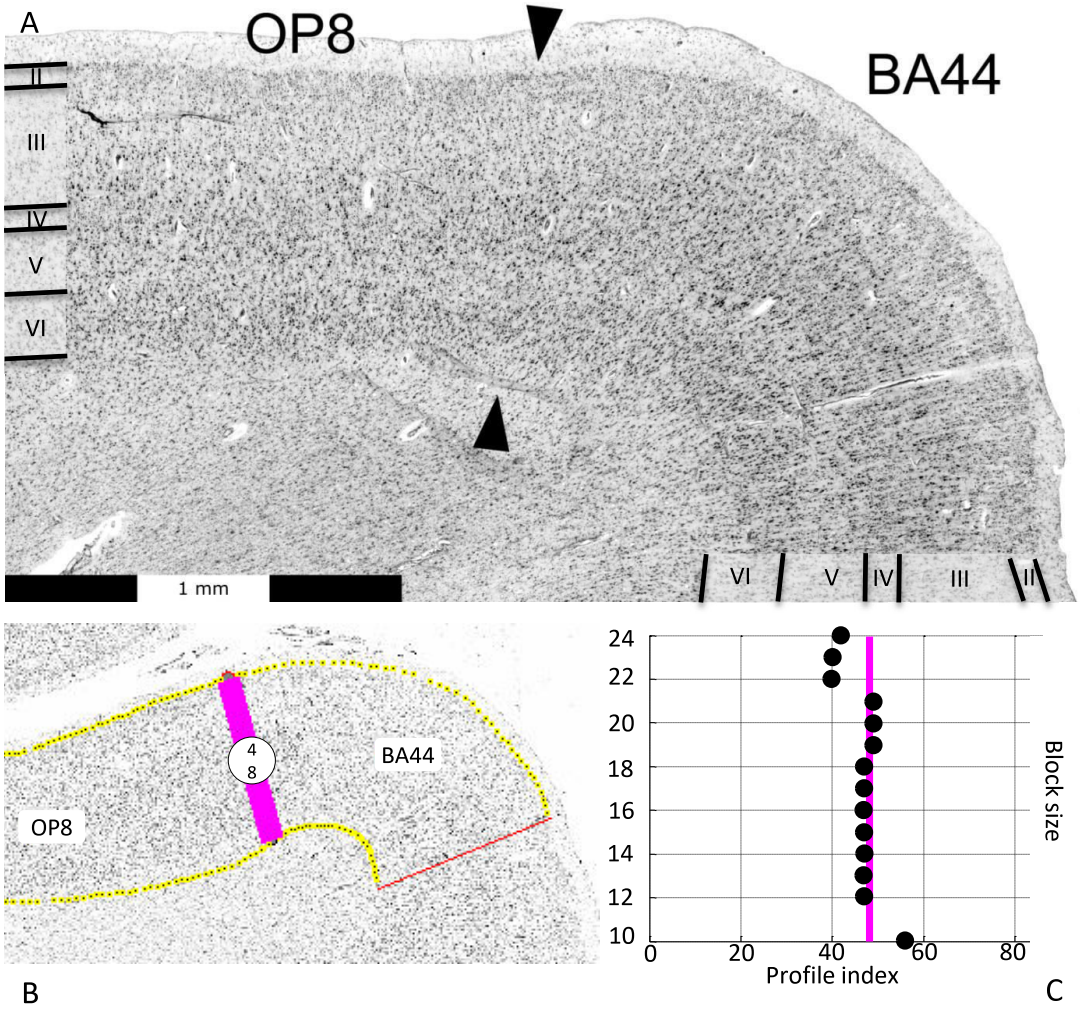

Fig. 4: Cytoarchitectonic border of OP8 and BA44 (A) with automatic border detection and dot blot illustrating the position of significant peaks (profile index) plotted against the block size

Roman numbers mark the laminae. Scale 1 mm per third. Notice that lamina III and V are less dense in OP8. Lamina IV is well visible in both areas, both areas are dysgranular. The transition of lamina VI to the white matter is more sharp in OP8. Lamination and visibility of columns are less distinct in OP8. **(B)** Inverted GLI image after automatic border detection. Significant borders are shown as pink lines, together with the corresponding profile number, at which the border is found. **(C)** Dot blot with block sizes (ordinate) and profile index (abscissa). Dots indicate the profile index, at which the Mahalanobis distance was significant.

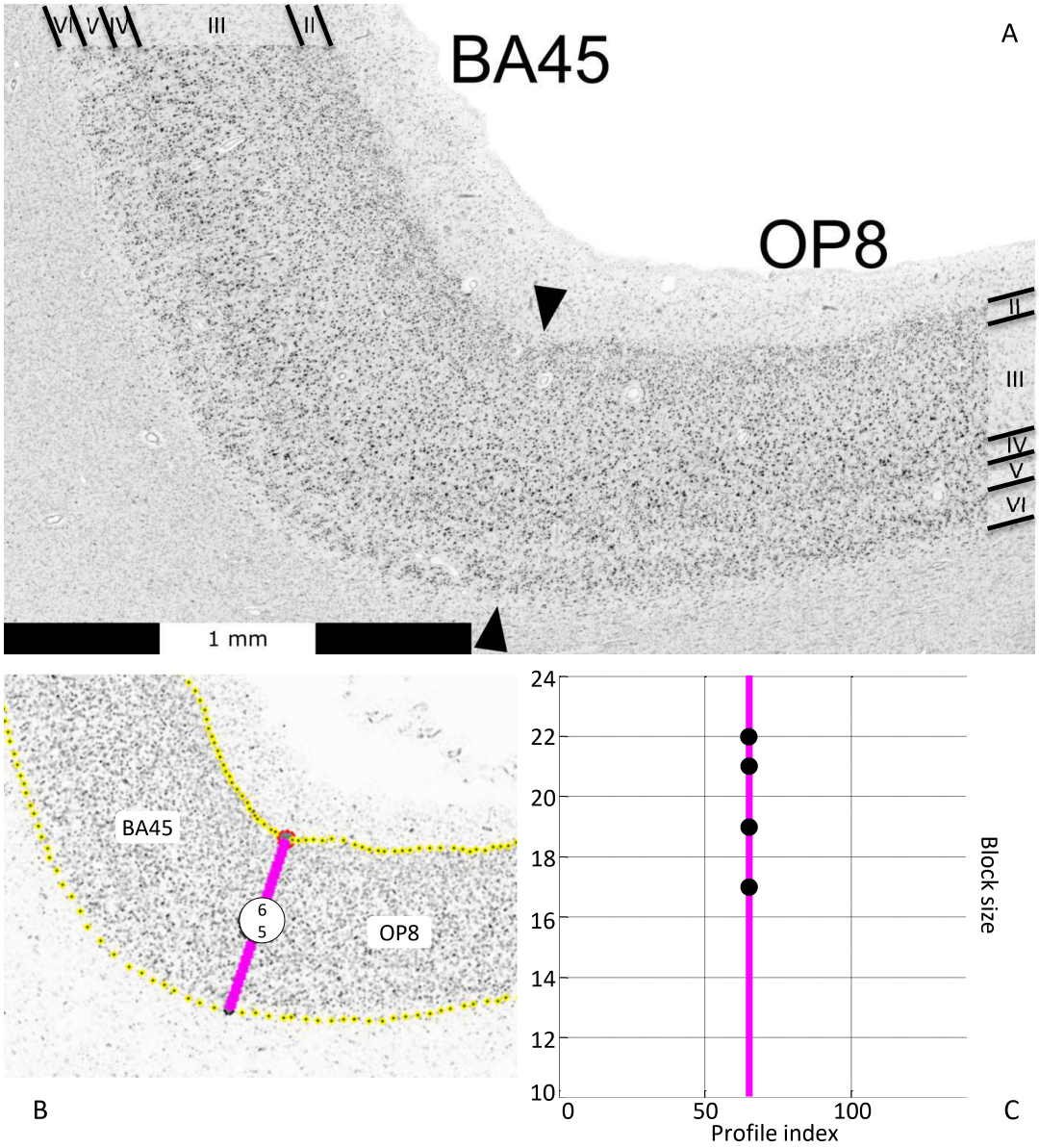

Fig. 5: Cytoarchitectonic border of OP8 and BA45 (A) with automatic border detection and dot blot illustrating the position of significant peaks (profile index) plotted against the block size

Roman numbers mark the laminae. Scale 1 mm per third. Notice that lamina III is less dense in OP8, while pyramidal cells are bigger and more prominent in BA45. Lamina IV is more narrow, less dense and less interspersed with pyramidal cells in OP8. Lamination and visibility of columns are less distinct in OP8. **(B)** Inverted GLI image after automatic border detection. Significant borders are shown as pink lines, together with the corresponding profile number, at which the border is found. **(C)** Dot blot with block sizes (ordinate) and profile index (abscissa). Dots indicate the profile index, at which the Mahalanobis distance was significant.

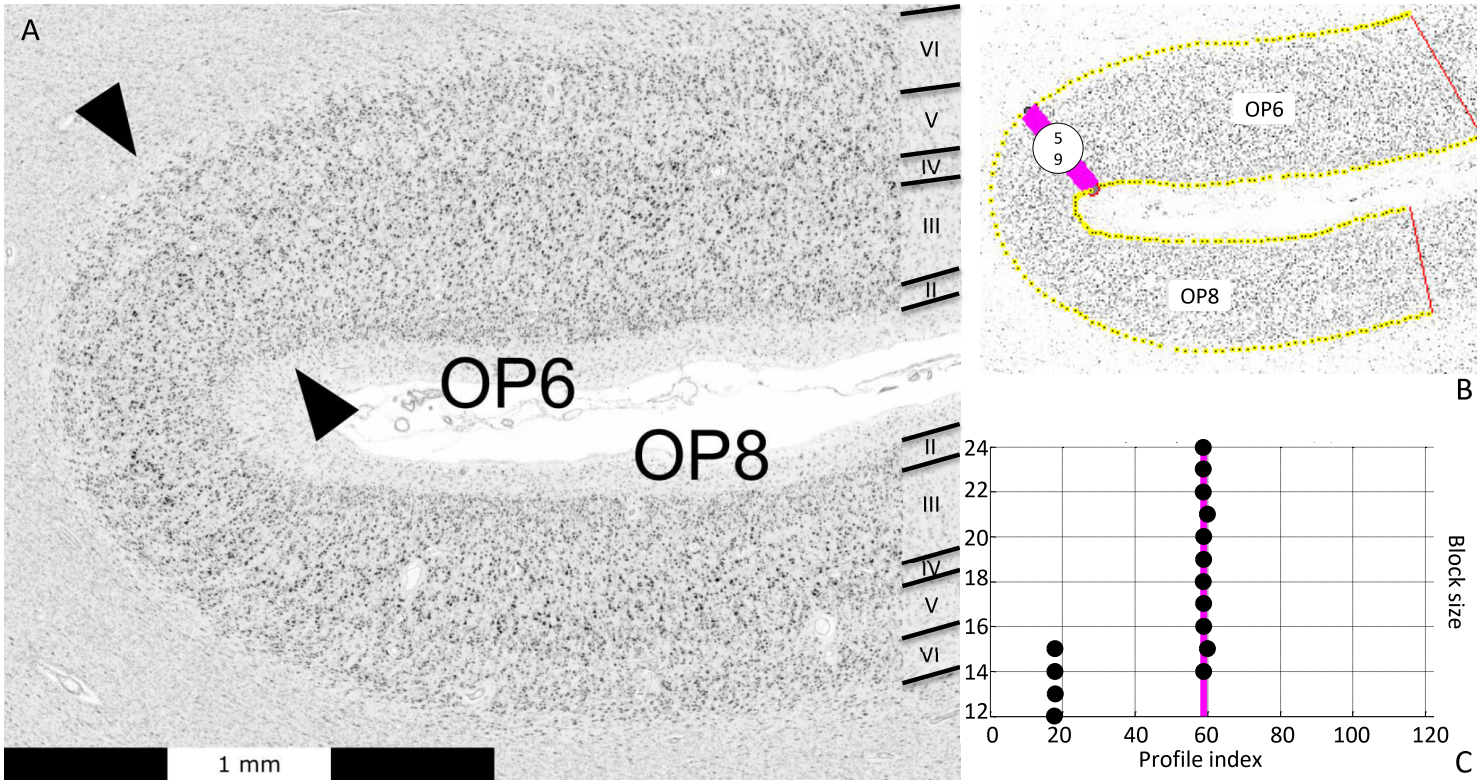

Fig. 6: Cytoarchitectonic border of OP8 and OP6 (A) with automatic border detection and dot blot illustrating the position of significant peaks (profile index) plotted against the block size

Roman numbers mark the laminae. Scale 1 mm per third. Notice that lamina II is less dense in OP8. Lamina IV is less dense in OP8, both areas are dysgranular. Lamina V is less dense and with less prominent pyramidal cells in upper V in OP8. **(B)** Inverted GLI image after automatic border detection. Significant borders are shown as pink lines, together with the corresponding profile number, at which the border is found. **(C)** Dot blot with block sizes (ordinate) and profile index (abscissa). Dots indicate the profile index, at which the Mahalanobis distance was significant. There was no significant border found at profile 19.

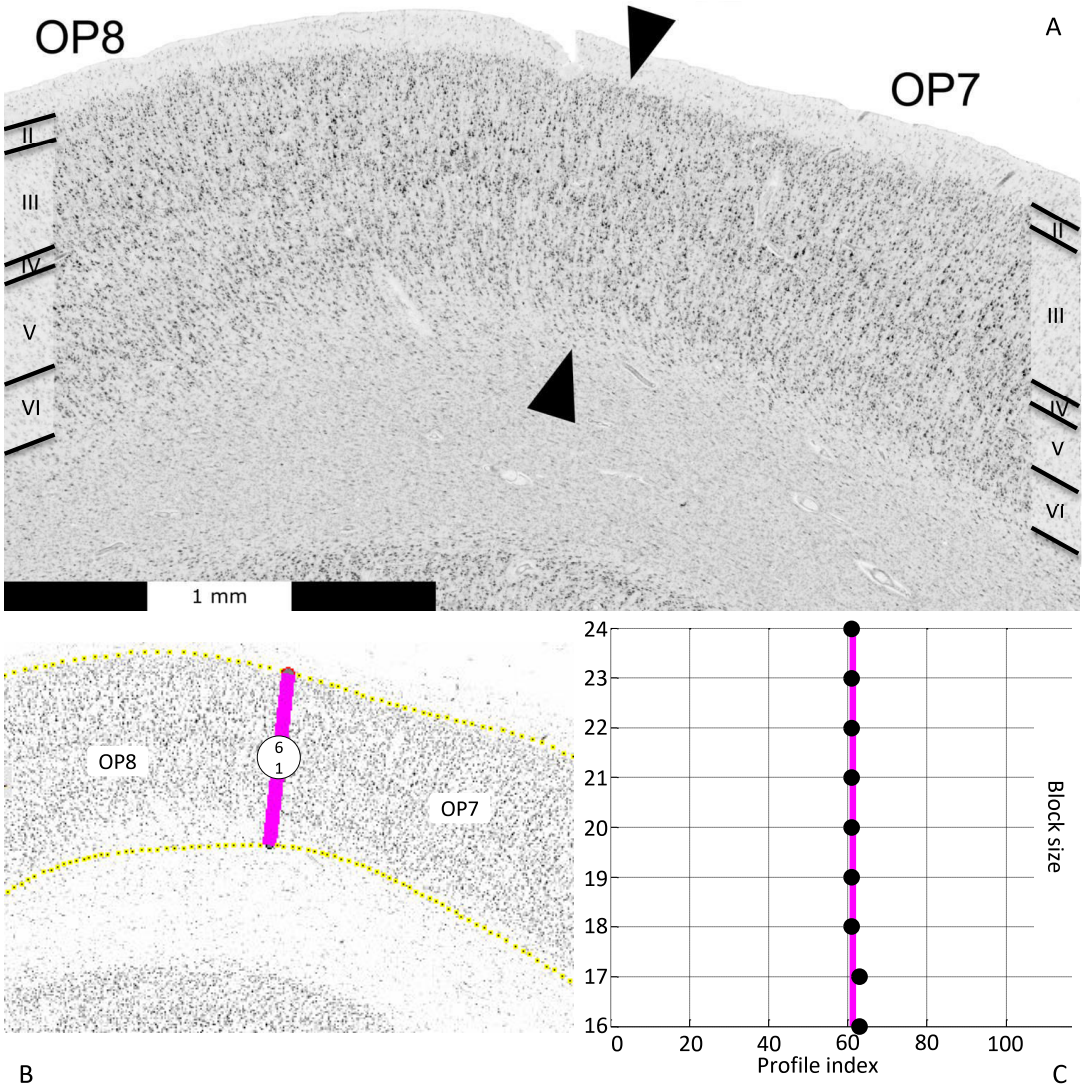

Fig. 7: Cytoarchitectonic border of OP8 and OP7 (A) with automatic border detection and dot blot illustrating the position of significant peaks (profile index) plotted against the block size

Roman numbers mark the laminae. Scale 1 mm per third. Notice that lamina II is less dense in OP8. Deep lamina III has less prominent pyramidal cells in OP8. Lamina IV is slightly less dense in OP8, both areas are dysgranular. Upper lamina V has less prominent pyramidal cells and mid V is less dense in OP8. Visibility of columns is less obvious in OP8. **(B)** Inverted GLI image after automatic border detection. Significant borders are shown as pink lines, together with the corresponding profile number, at which the border is found. **(C)** Dot blot with block sizes (ordinate) and profile index (abscissa). Dots indicate the profile index, at which the Mahalanobis distance was significant.

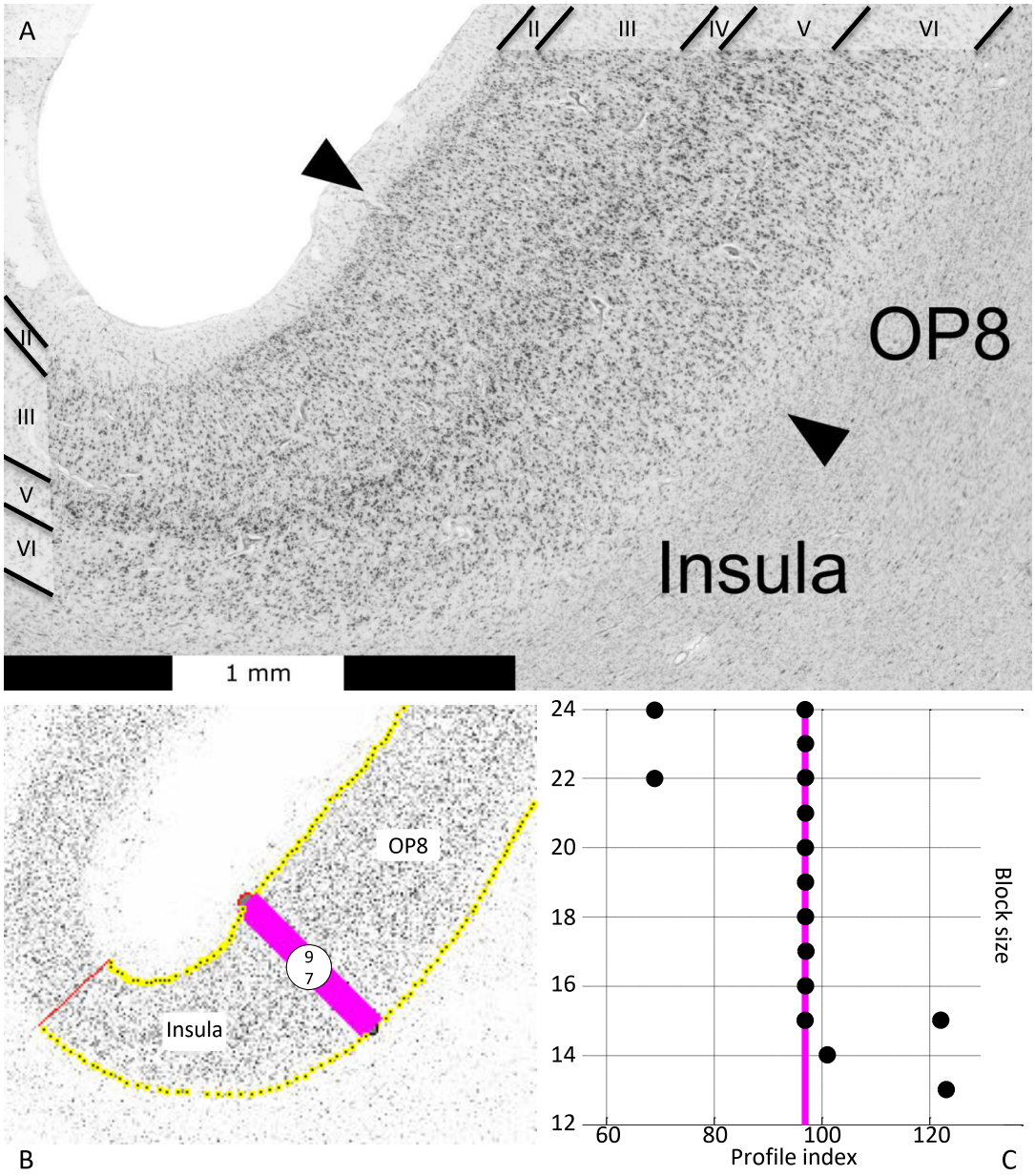

Fig. 8: Cytoarchitectonic border of OP8 and the insula (A) with automatic border detection and dot blot illustrating the position of significant peaks (profile index) plotted against the block size

Roman numbers mark the laminae. Scale 1 mm per third. Notice that lamina II is more dense in OP8, while almost not distinguishable in the insula. Lamina III has more prominent pyramidal cells in deep III in OP8, while there are almost none in the insula. OP8 is dysgranular, the insula is almost agranular. Lamination and visibility of columns is more distinct in OP8. **(B)** Inverted GLI image after automatic border detection. Significant borders are shown as pink lines, together with the corresponding profile number, at which the border is found. **(C)** Dot blot with block sizes (ordinate) and profile index (abscissa). Dots indicate the profile index, at which the Mahalanobis distance was significant. There was no significant border at profile 69 and 122.

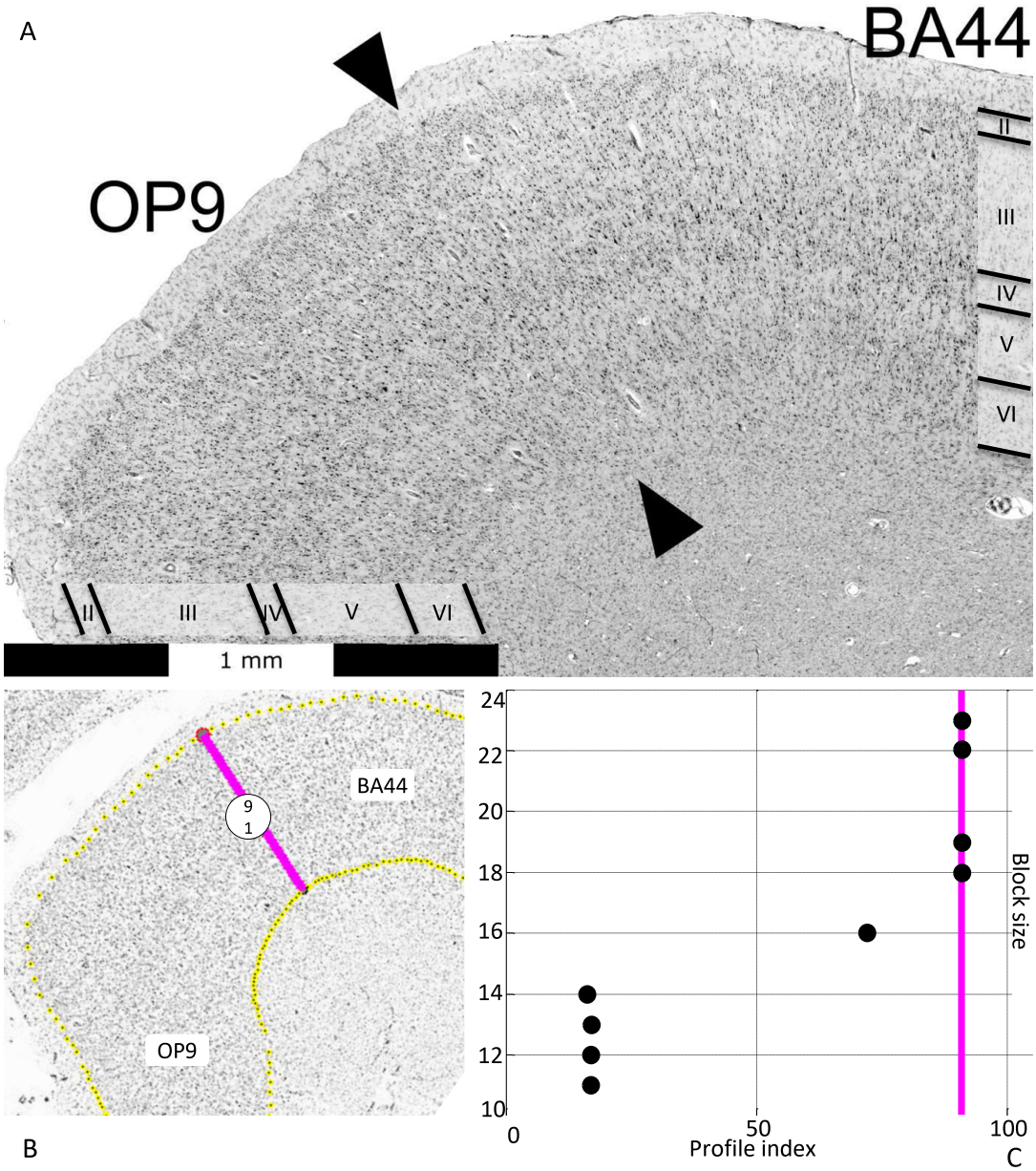

Fig. 9: Cytoarchitectonic border of OP9 and BA44 (A) with automatic border detection and dot blot illustrating the position of significant peaks (profile index) plotted against the block size

Roman numbers mark the laminae. Scale 1 mm per third. Notice that lamina III is more dense in OP9, but pyramidal cells are bigger and more prominent in BA44. Lamina IV is less dense in OP9. Lamina V is slightly less dense in OP9, both areas have prominent pyramidal cells in upper V. Almost no lamination and visibility of columns in OP9 in contrast to BA44. **(B)** Inverted GLI image after automatic border detection. Significant borders are shown as pink lines, together with the corresponding profile number, at which the border is found. **(C)** Dot blot with block sizes (ordinate) and profile index (abscissa). Dots indicate the profile index, at which the Mahalanobis distance was significant. There was no significant border at profile 20.

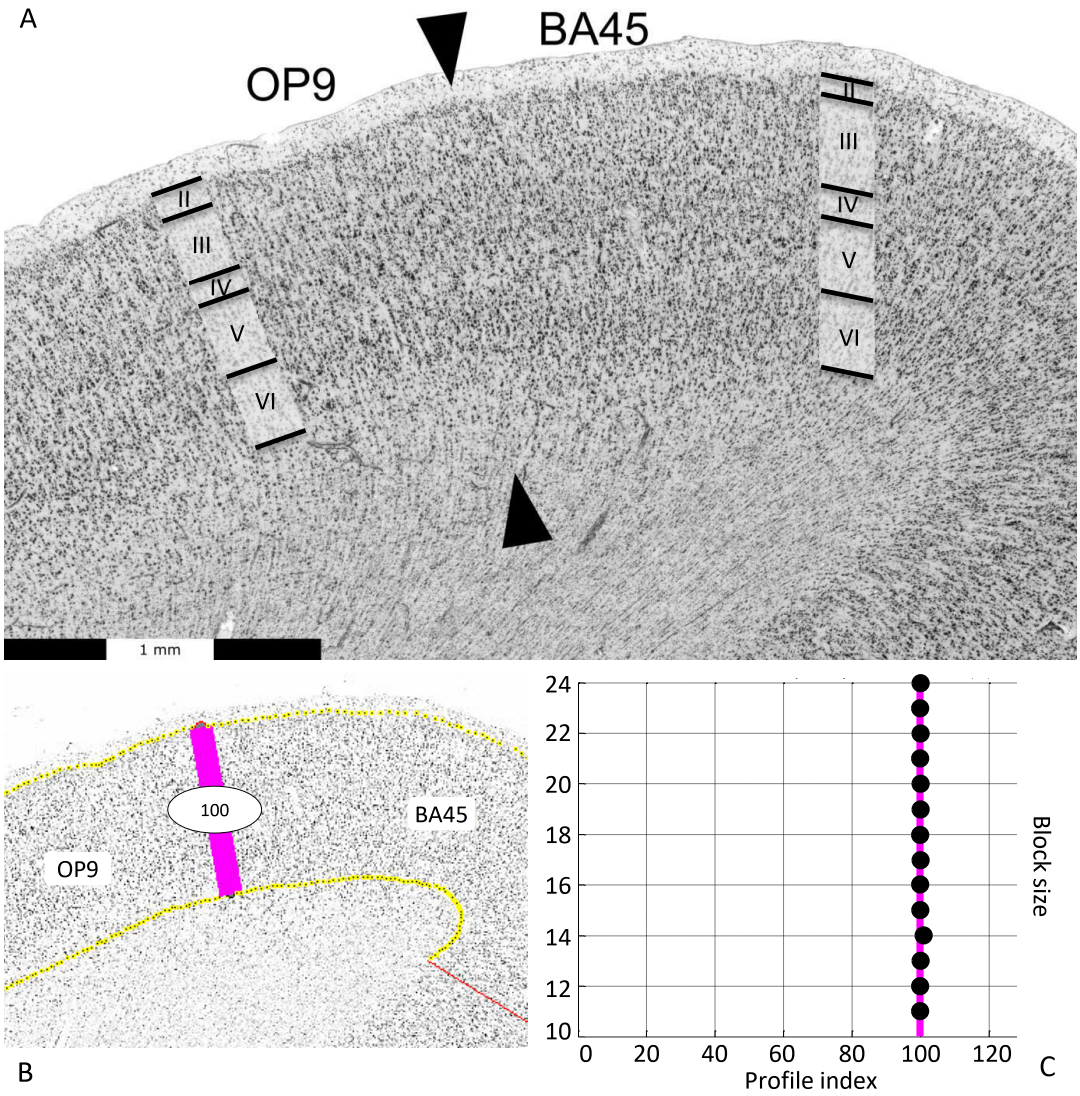

Fig. 10: Cytoarchitectonic border of OP9 and BA45 (A) with automatic border detection and dot blot illustrating the position of significant peaks (profile index) plotted against the block size

Roman numbers mark the laminae. Scale 1 mm per third. Notice that lamina III is more consistently dense in OP9, while pyramidal cells are bigger and more prominent in BA45. Lamina IV is less dense in OP9, while well visible and dense in BA45 being a granular area. Lamina V is less dense in OP9 with less prominent pyramidal cells in upper V. Lamination and visibility of columns is almost non-existent in OP9 while well visible in BA45. **(B)** Inverted GLI image after automatic border detection. Significant borders are shown as pink lines, together with the corresponding profile number, at which the border is found. **(C)** Dot blot with block sizes (ordinate) and profile index (abscissa). Dots indicate the profile index, at which the Mahalanobis distance was significant.

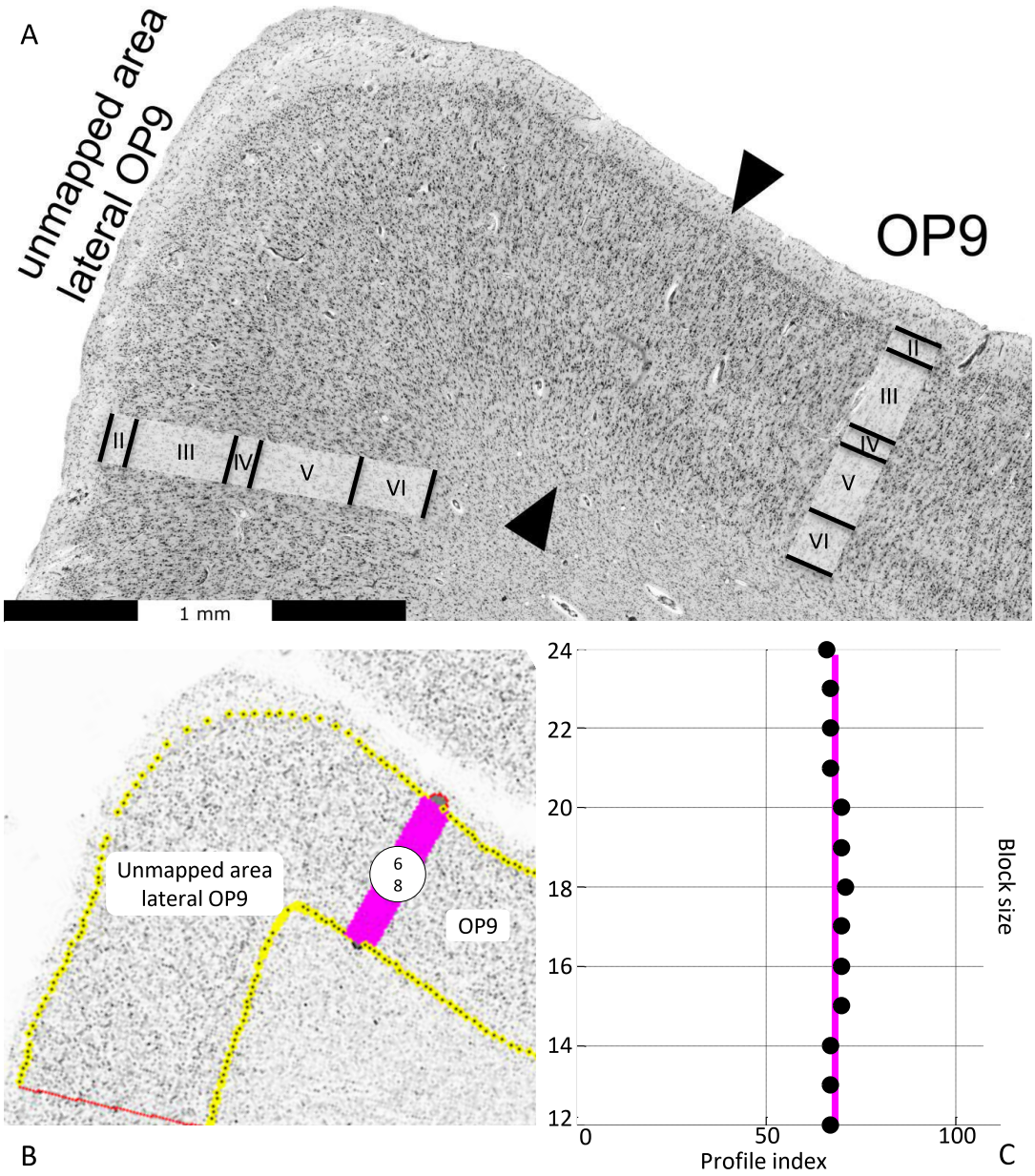

Fig. 11: Cytoarchitectonic border of OP9 and unmapped area lateral of OP9 (A) with automatic border detection and dot blot illustrating the position of significant peaks (profile index) plotted against the block size

Roman numbers mark the laminae. Scale 1 mm per third. Notice that lamina II is more dense in OP9. Pyramidal cells are bigger and more prominent in the latearl area. Lamina IV is thin in both areas. Lamina V is less dense in OP9, both lack prominent pyramidal cells in upper V. Lamina VI is more dense in OP9 with a sharper transition to the white matter. **(B)** Inverted GLI image after automatic border detection. Significant borders are shown as pink lines, together with the corresponding profile number, at which the border is found. **(C)** Dot blot with block sizes (ordinate) and profile index (abscissa). Dots indicate the profile index, at which the Mahalanobis distance was significant.

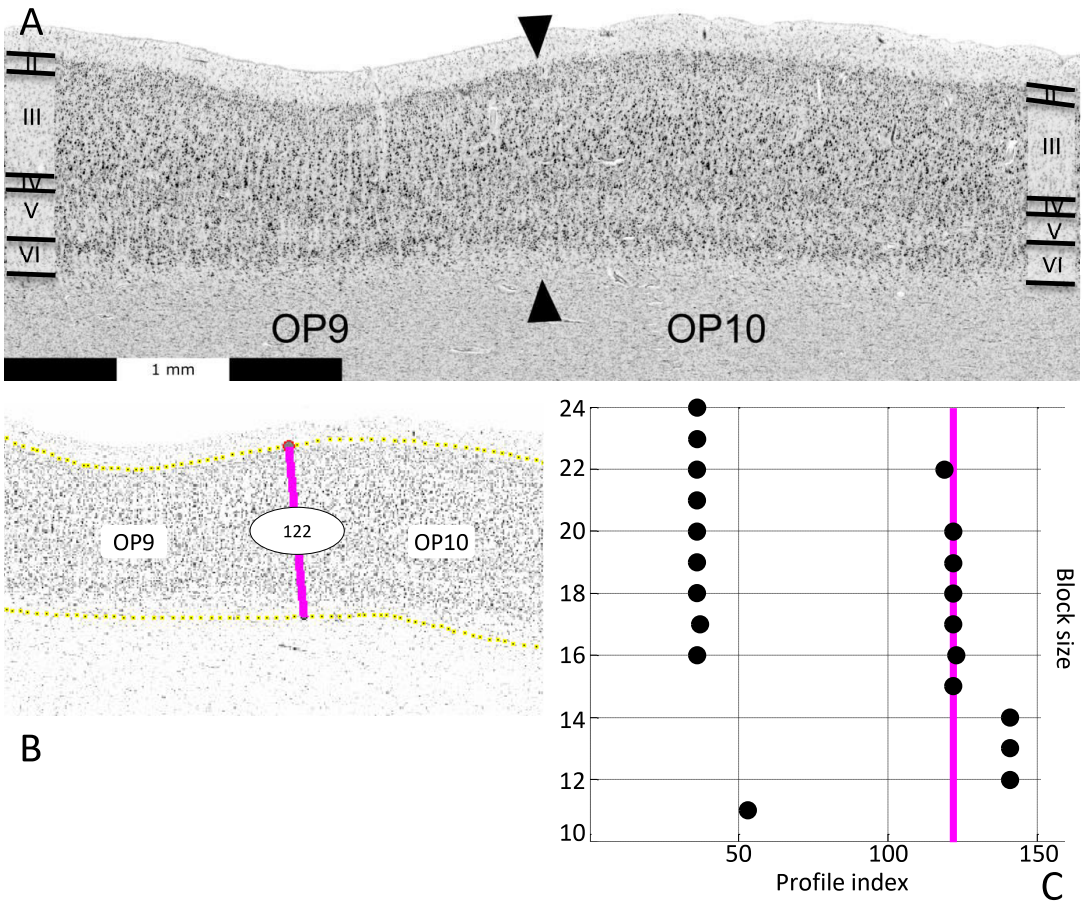

Fig. 12: Cytoarchitectonic border of OP9 and OP10 (A) with automatic border detection and dot blot illustrating the position of significant peaks (profile index) plotted against the block size

Roman numbers mark the laminae. Scale 1 mm per third. Notice that mid lamina III is more dense and pyramidal cells in deep III are more prominent in OP9. While both areas are dysgranular, lamina IV is more visible as a ribbon in OP10. Lamina V is more dense in OP9 with less slightly prominent pyramidal cells in upper V in OP9 (thus the impression of a ribbon by lamina IV in OP10). Lamina VI is more dense with a slightly more sharp transition to the white matter in OP9. **(B)** Inverted GLI image after automatic border detection. Significant borders are shown as pink lines, together with the corresponding profile number, at which the border is found. **(C)** Dot blot with block sizes (ordinate) and profile index (abscissa). Dots indicate the profile index, at which the Mahalanobis distance was significant. Significant border at profile 36 (lateral border of OP9) not in this display.

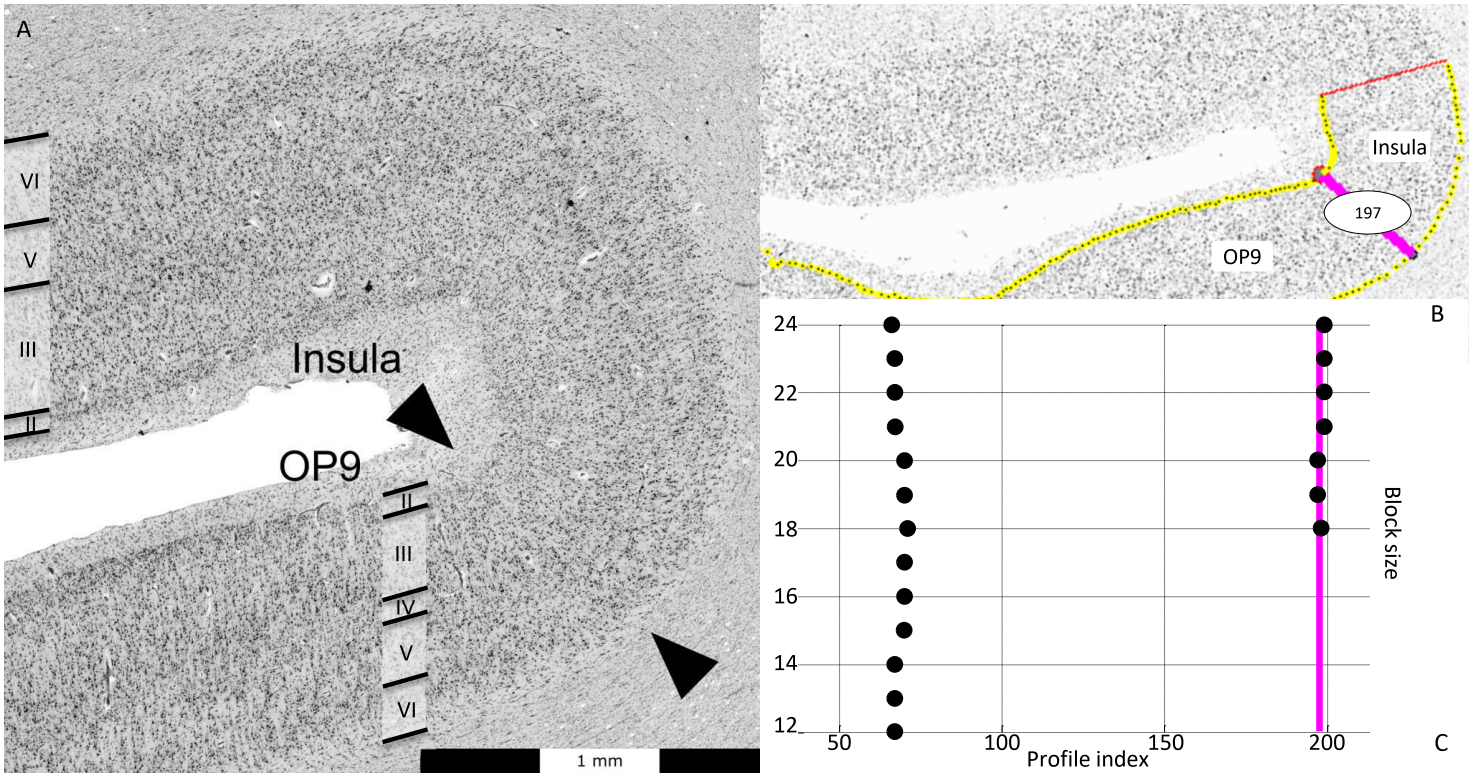

Fig. 13: Cytoarchitectonic border of OP9 and the insula (A) with automatic border detection and dot blot illustrating the position of significant peaks (profile index) plotted against the block size.

Roman numbers mark the laminae. Scale 1 mm per third. Notice that deep lamina III has prominent pyramidal cells in OP9, while there are almost none in the insula. Lamina IV is not visible in the insula, while OP9 is a dysgranular area. Lamina V is less dense in OP9. Lamina VI is more dense in OP9 with blurred transition to the white matter. **(B)** Inverted GLI image after automatic border detection. Significant borders are shown as pink lines, together with the corresponding profile number, at which the border is found. **(C)** Dot blot with block sizes (ordinate) and profile index (abscissa). Dots indicate the profile index, at which the Mahalanobis distance was significant. Significant border at profile 68 (lateral border of OP9) not in this display.

Correlation with anatomical landmarks and neighbouring areas

OP8 is located more caudally than area OP9 in the frontal operculum. They both primarily follow the depth of the lateral fissure, lateral to the insular cortex. OP8 is medially directly adjacent to BA44, OP9 to BA45 respectively. In one brain, OP9 is laterally bordering to a yet unmapped area for a distance of 2.4 mm (see **Figure 11)**. OP8 does not directly border previously defined OP1-4 (Eickhoff, Schleicher et al., 2006), which are situated in the parietal operculum. The gap in between comprises two areas of current further research, i.e. OP6 and OP7. OP8 caudolaterally adjoins both OP6 and OP7. In addition to areas OP6 and OP7, there is a further area rostrally bordering OP9, which was named OP10 and is alike subject of further research. Both OP8 and OP9 are medially adjoined by the insular cortex. They don't exceed the curvature of the transition of the opercular gyrus and the insular gyrus. The insular cortex rostroventrally medially adjoining OP9 is partially the anterior dorsal insula (Iad7). Except for 2 sections in all 10 investigated brains, OP8 and OP9 never reached the free lateral brain surface. In these two sections, left OP8 is slightly superficial, but still inside the sulcus on a more spacious part of the gyrus. Indirect landmarks can be used to estimate the extent of both areas from a lateral superficial view (see **Table 3, Figure 14**).

area	border location	landmark	area	border location	landmark
OP8 left	caudal	iprs	OP8 right	caudal	iprs
OP8 left	rostral	alf/hlf	OP8 right	rostral	alf/hlf
OP9 left	caudal	ds/alf	OP9 right	caudal	alf/iprs
OP9 left	rostral	end of ts/ds	OP9 right	rostral	end of ts/ds

Table 3: Indirect landmarks for estimation of the extent of OP8 and OP9 from lateral view of an intact brain surface

The landmarks are meant to be the projected borders of the areas, i.e. do not claim to be direct correlates of the borders, but their appearance in transversal plain roughly correlates to the extent of the area. Note, that the caudal surrogate border of right OP8 (iprs) in this table is different to that shown in **Figure 2** (central sulcus), as this table is based on comparison of all 10 investigated brains and lists those borders most frequently found. *alf*, ascending branch of the lateral fissure; *ds*, diagonal sulcus; *hlf*, horizontal branch of the lateral fissure; *iprs*, inferior precentral sulcus; *ts*, triangular sulcus.

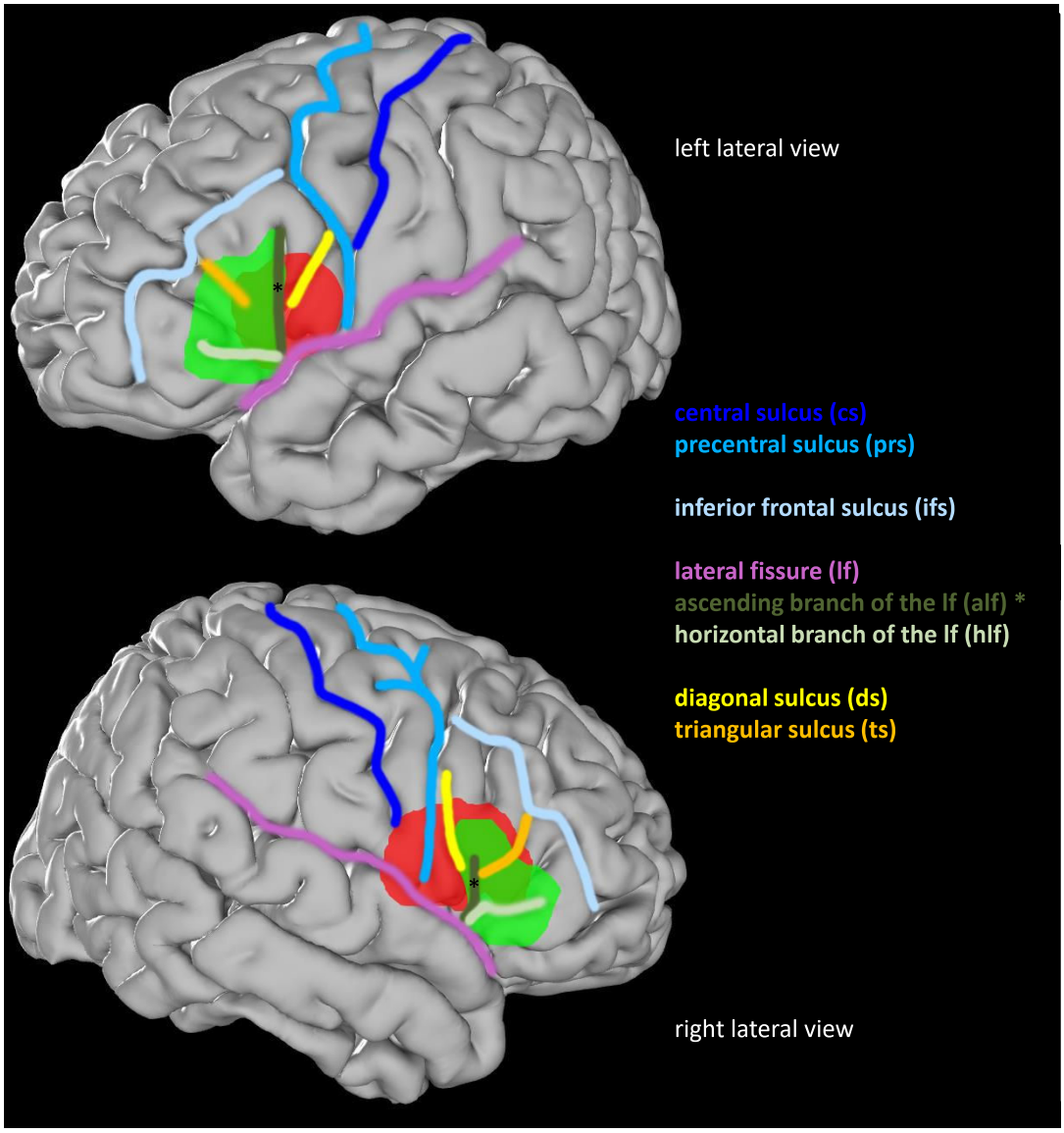

Fig. 14: Reference brain from a lateral view showing OP8 and OP9 in their extent according to the full probability map ranging from 0% to 100%

Sulci are colour-coded according to the labelling by Tzourio-Mazoyer et al., 2002 – divergence in right lateral view, where we name the vertical sulcus rostral of the precentral sulcus as triangular sulcus and not as part of the ascending branch of the lateral fissure. The triangular sulcus is not named in that publication. Where the areas seem to cross over to the temporal gyrus, this is due to superposition, as they both solely extent in the depth of the circular insular sulcus and do not meet the free surface.

Volumes of OP8 and OP9

In 50% of the 10 investigated brains, OP8 is larger in the left hemisphere than in the right hemisphere. There were substantial variations in volume, especially in

OP8 of the left hemisphere, ranging from 209 mm³ up to 1084 mm³. Comparing shrinkage corrected mean areal volumes of all brains, OP8 is of larger volume in the right hemisphere than in the left hemisphere. Yet, these volume differences did not reach significance after normalization ($p>0.05$). In 60% of all individual brains, left OP9 is larger than the contralateral area. This is approved by comparison of the bilateral mean areal volumes. Comparable to OP8, these differences also did not reach significance after normalization ($p>0.05$).

The mean total volume of OP8 is about 1.49 times larger than OP9. For the volumes of area OP8 and OP9 in each investigated brain after volume correction, as well as the median volumes of both areas, see **Table 4 A and B**.

		Shrinkage corrected volumes [mm³]				
Brain code	**Sex**	**Shrinkage factor**	**OP8 left**	**OP8 right**	**OP9 left**	**OP9 right**
1	w	1.7	645	563	320	297
2	m	2.0	590	866	703	370
3	m	2.0	1084	1083	653	420
4	m	1.9	589	929	623	646
5	w	2.2	553	744	913	579
6	m	2.5	1066	1055	713	263
7	m	2.3	764	335	321	359
8	w	1.9	748	591	511	462
9	w	1.5	209	919	665	714
10	w	1.7	565	840	176	199

Table 4A: Corrected volumes of OP8 and OP9 of each hemisphere in each of the 10 investigated brains after shrinkage correction

Based on the individual shrinkage factor of each brain. *w*, female; *m*, male

area	mean volume [mm³]	SD [±]
OP8 left	681	256
OP8 right	792	236
OP8 total	737	247
OP9 left	560	225
OP9 right	431	169
OP9 total	495	205

Table 4B: Mean areal volumes of OP8 and OP9

SD, standard deviation

There were no significant differences found ($p>0.05$) after applying pairwise permutation test for comparison of volume differences regarding region and hemisphere. When normalized as percentage of the standardized total brain volume, left OP8 takes 0.53% vs. 0.63% on the right hemisphere, resulting in $p=0.25$. Left OP9 takes 0.45% vs. 0.35% on the right, thus $p=0.1$. When comparing the areal volumes regarding gender for single hemispheres or in between those, as well as gender dependence of total areal volume in both hemispheres, there were also no significant differences measured ($p>0.05$).

Cytoarchitectonic dependency by hierarchical cluster analysis

The dendrogram of the hierarchical cluster analysis (see **Figure 15**) shows a high similarity of areas OP8 and OP9, as they cluster together. Furthermore, BA44 and BA45 build a cluster. BA47, which was included in this analysis as an area related to and caudally bordering BA45, builds a separate group. Yet, the smaller Euclidean distance of the frontal opercular areas to BA47 compared to the “classical Broca’s areas” BA44 and BA45 suggests a higher cytoarchitectonic similarity despite the lack of a true cortical border.

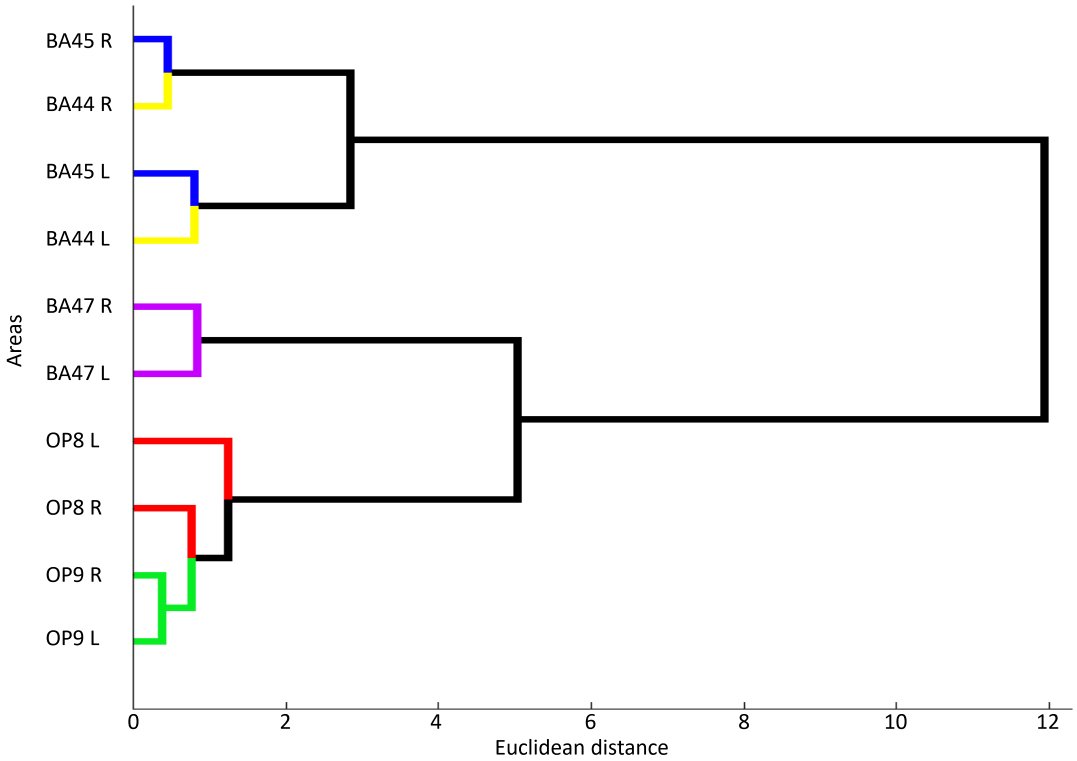

Fig. 15: Dendrogram of the hierarchical cluster analysis

Areas **OP8** and **OP9** and their already delineated adjacent areas **BA44**, **BA45** and **BA47**, are partitioned by their respective hemispheres (L = left hemisphere, R = right hemisphere).

The smaller the Euclidean distance, the higher the cytoarchitectonic similarity. Notice the frontal opercular areas OP8 and OP9 clustering together. Furthermore "classical Broca's areas" BA44 and BA45 build a separate cluster. BA47, while not directly adjacent to OP8 and OP9, has a higher cytoarchitectonic similarity to the frontal opercular areas expressed in the smaller Euclidean distance than Broca's areas.

Probability in stereotaxic space

Probabilistic maps represent the colour-coded areal overlapping and thus indicate inter-individual variability. Red colour denotes maximum probability of finding the specific area in that exact voxel. The colour scale ranges over green for medium probability to purple for lowest probability. See **Figure 16** for the probability map of OP8 and **Figure 17** for OP9.

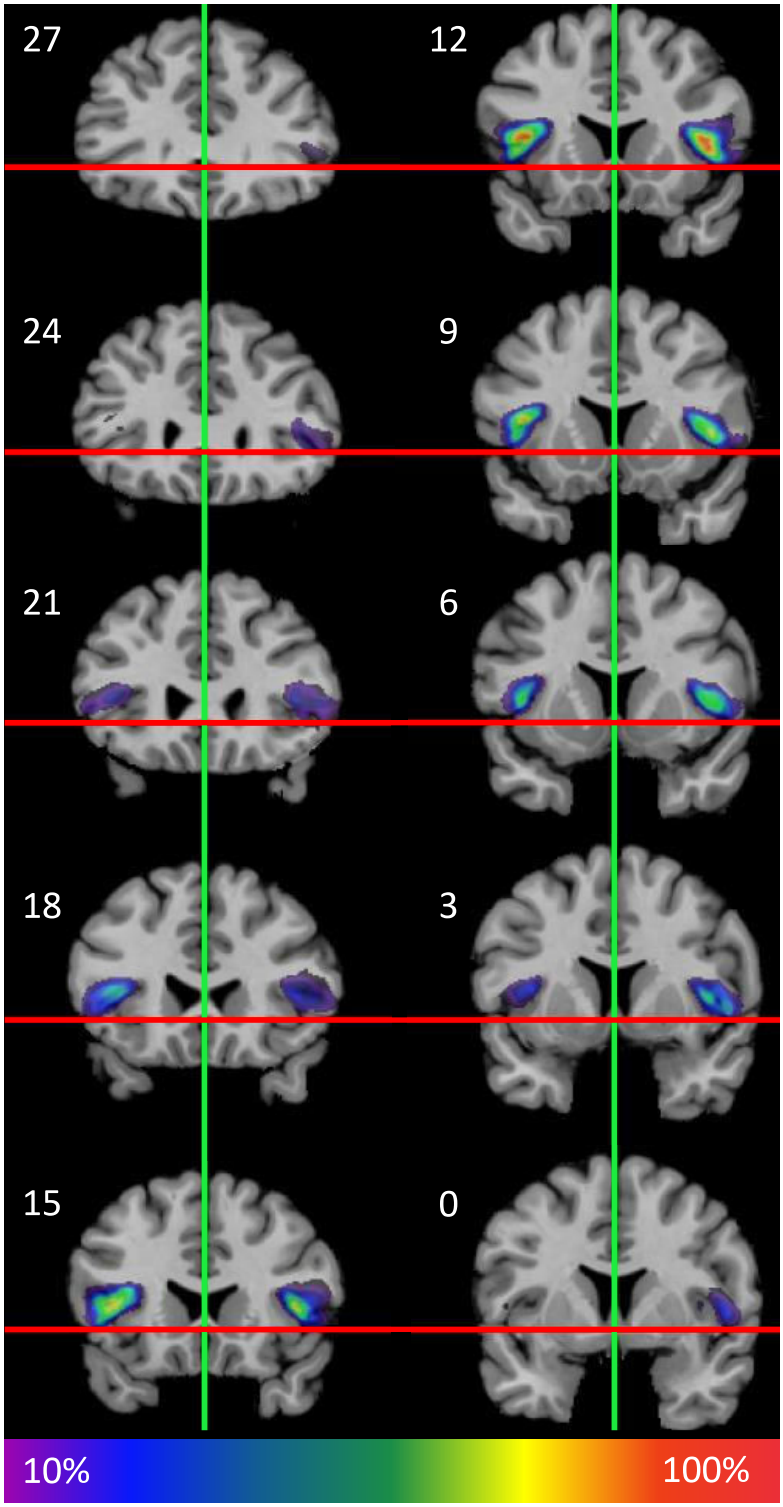

Fig. 16: Probability map of area OP8 normalized to the MNI reference brain in coronal sections

Colours code the probability of finding the area in that exact voxel, originating from the overlapping of the area in all 10 investigated brains. Red marks highest probability (100%), purple marks lowest probability (10%). White numbers indicate y-coordinates in MNI space, red and green lines cross in the zero-point.

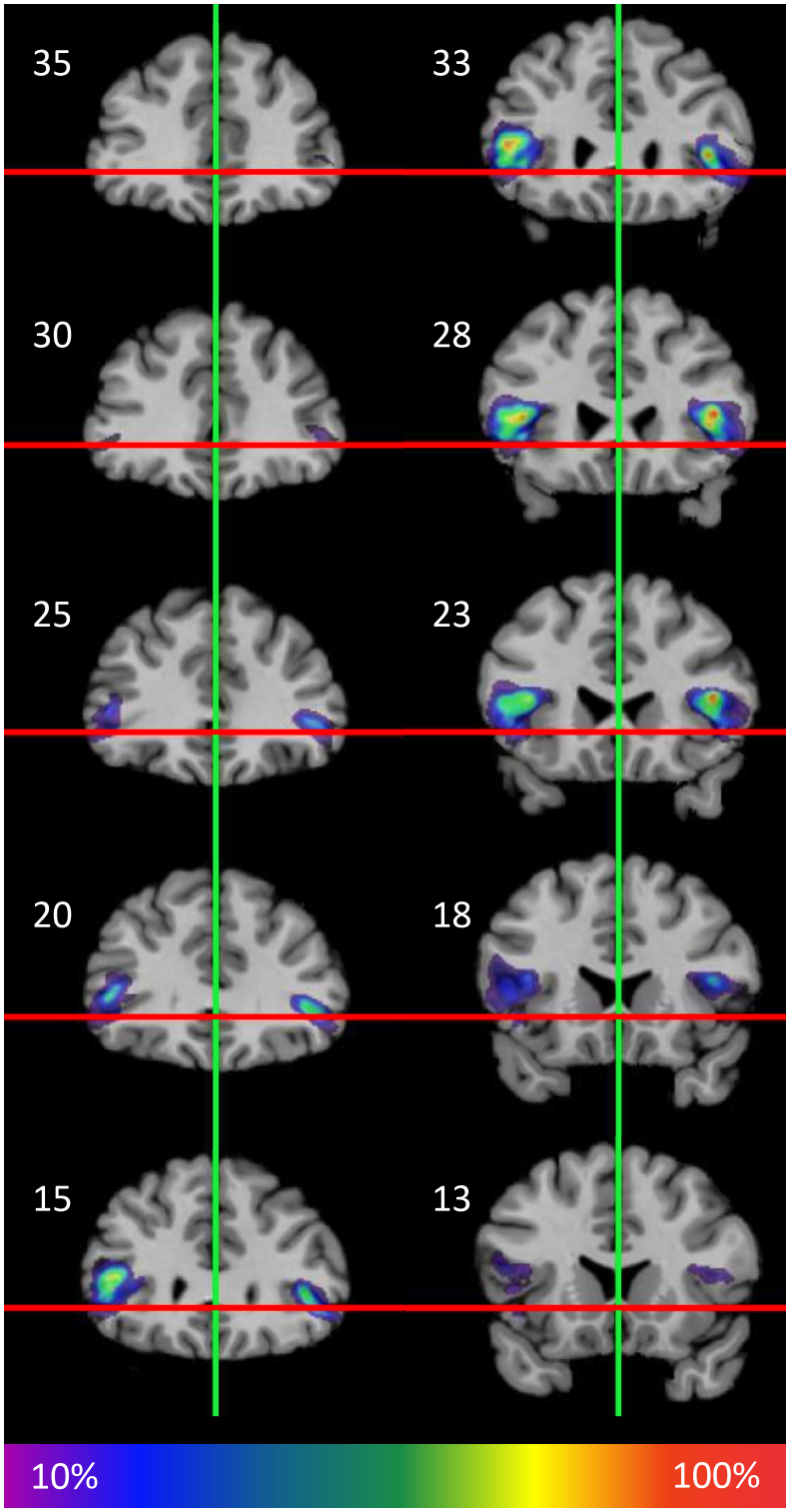

Fig. 17: Probability map of area OP9 normalized to the MNI reference brain in coronal sections

Colours code the probability of finding the area in that exact voxel, originating from the overlapping of the area in all 10 investigated brains. Red marks highest probability (100%), purple marks lowest probability (10%). White numbers indicate y-coordinates in MNI space, red and green lines cross in the zero-point.

The maximum probability map combines the individual probabilistic maps and assigns a specific cortical area to each voxel where it can be found with maximum likelihood. For the full probability 3D render of OP8 and OP9 ranging from 0% to 100% probability, see **Figure 14**, where it was already shown to illustrate indirect anatomical landmarks for the extent of OP8 and OP9.

Based on the maximum probability map, the centres of gravity of both areas were calculated for both hemispheres. **Figure 18** shows the coordinates of these centres of gravity in MNI space, as well as in the Talairach and Tournoux space after transformation for easier comparison with the centres of gravity of activations as reported in functional studies.

OP8 left	Coordinates of the centre of gravity		
	x	y	z
MNI space	-42,47	19,57	1,90
Talairach space	-40,3	16,5	6,87

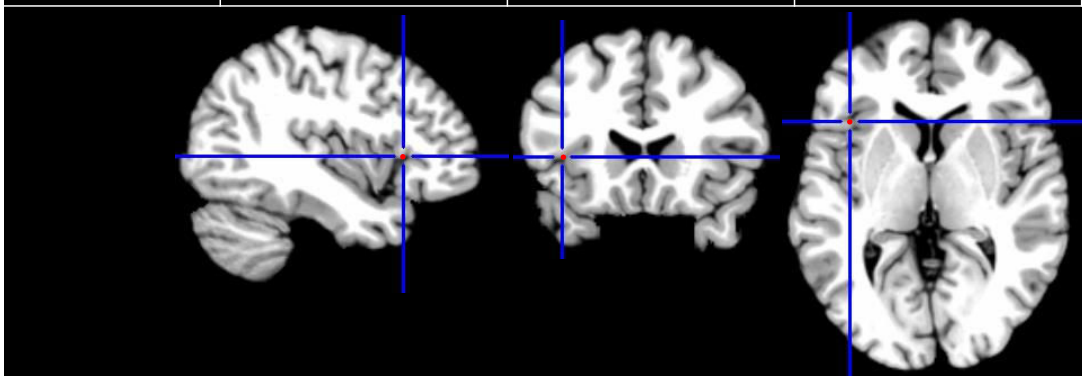

OP8 right	Coordinates of the centre of gravity		
	x	y	z
MNI space	43,61	17,67	0,22
Talairach space	39,38	14,47	6,51

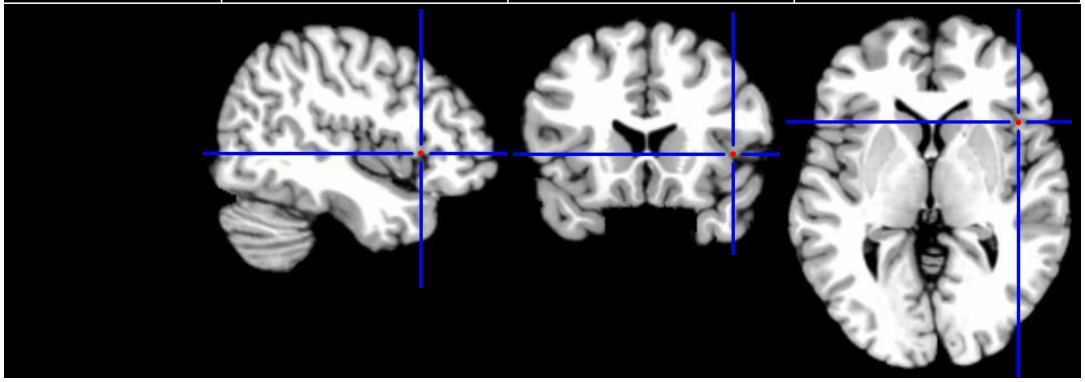

OP9 left	Coordinates of the centre of gravity		
	x	y	z
MNI space	-46,60	28,68	-0,45
Talairach space	-44,07	25,21	5,52

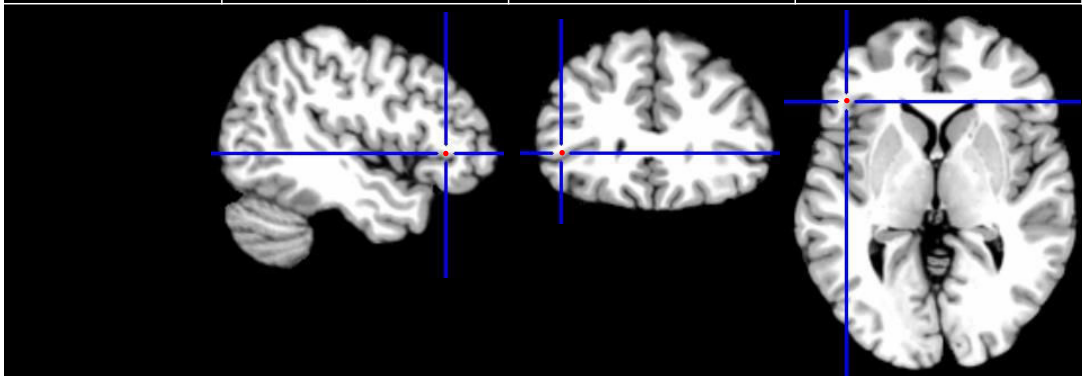

OP9 right	Coordinates of the centre of gravity		
	x	y	z
MNI space	43,79	28,99	-3,11
Talairach space	39,61	25,30	4,54

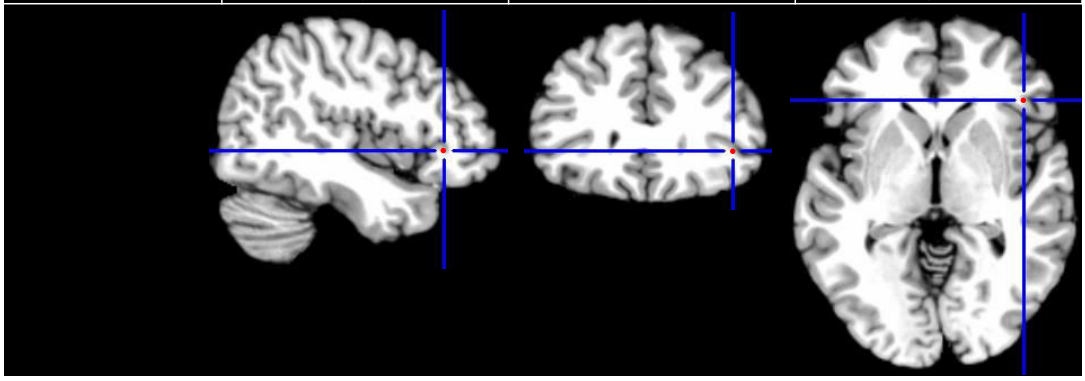

Fig. 18: Coordinates of the centres of gravity of OP8 and OP9 based on the maximum probability map, visualised in MNI space, and coordinates after conversion into the Talairach and Tournoux space

The MRI scans below each coordinate show the crosshair pointing at the centre of gravity in MNI space in a sagittal, coronal and horizontal plane on the colin27 template.

Functional attribution and co-activation analysis by meta-analytic connectivity modelling

The areal locations according to the probability maps were used as seed regions to investigate possible functions of the areas OP8 and OP9 by meta-analytic connectivity modelling (MACM). The results of this analysis for OP8 and OP9 regarding both hemispheres can be seen in **Figure 19** and **Figure 20**.

There are listed all relevant Behavioural Domains (BD) and Paradigm Classes (PC). The top row shows the most common BD, the bottom row shows the most common PC. The left column lists the likelihood ratio, that activity in the specific area produces the particular BD or PC. The right column lists the probability that executing the particular BD or PC will create activation in the specific area. Full coloured bars mark those items that remain after correction by false discovery rate (FDR) for multiple comparisons, while paled coloured bars mark the uncorrected items. The most significant conjunctions and contrasts of the BD and PC of OP8 and OP9 are shown in **Figure 21** and **Figure 22**.

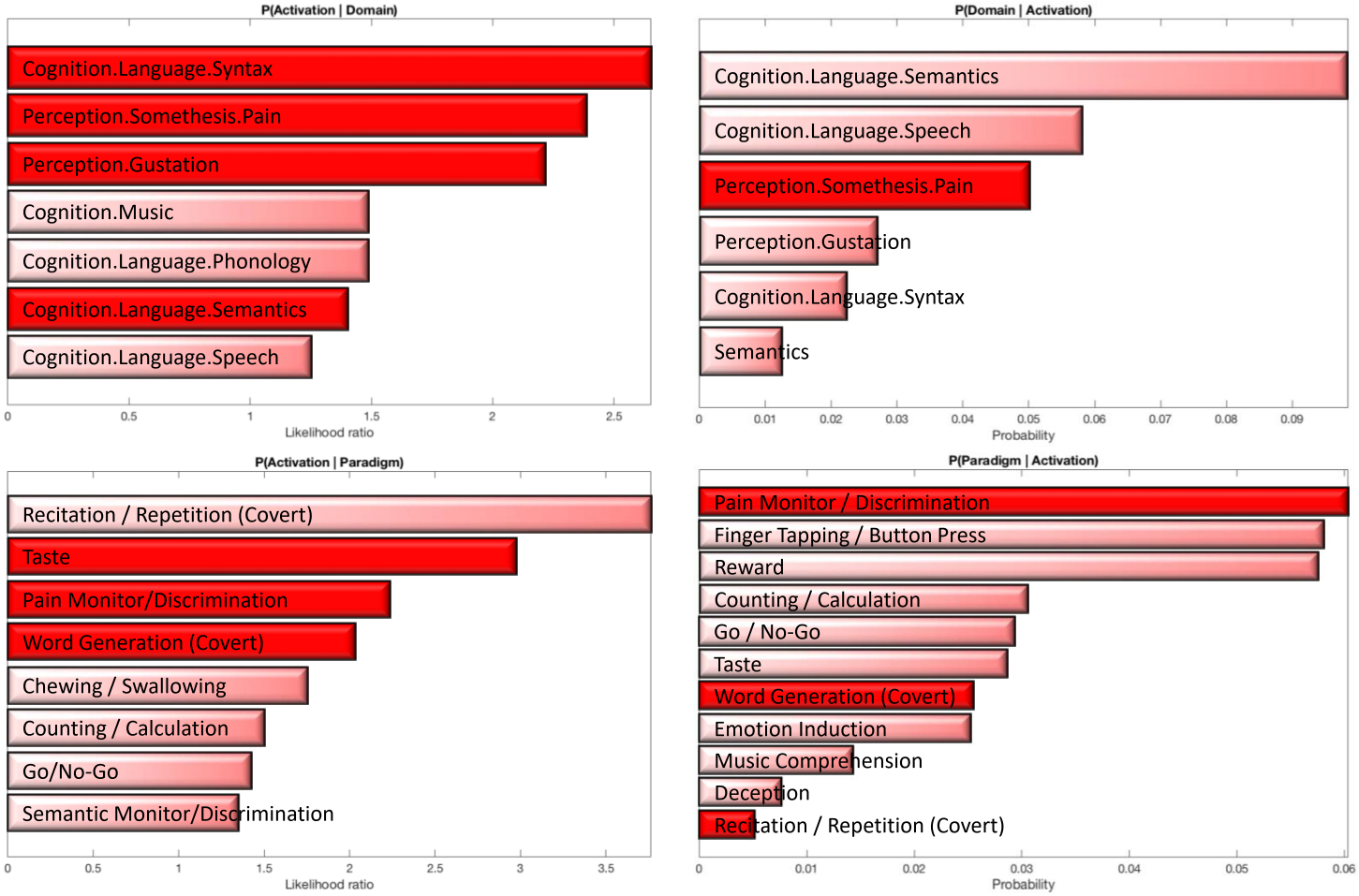

Fig. 19: Functional attribution of OP8 according to MACM analysis, regarding both hemispheres

Top row: most common BD; bottom row: most common PC; left column: likelihood ratio that activity in OP8 generates the BD/PC; right column: probability that the BD/PC will produce activation in OP8; full colour bars indicate remaining BD and PC after correction by FDR (false discovery rate).

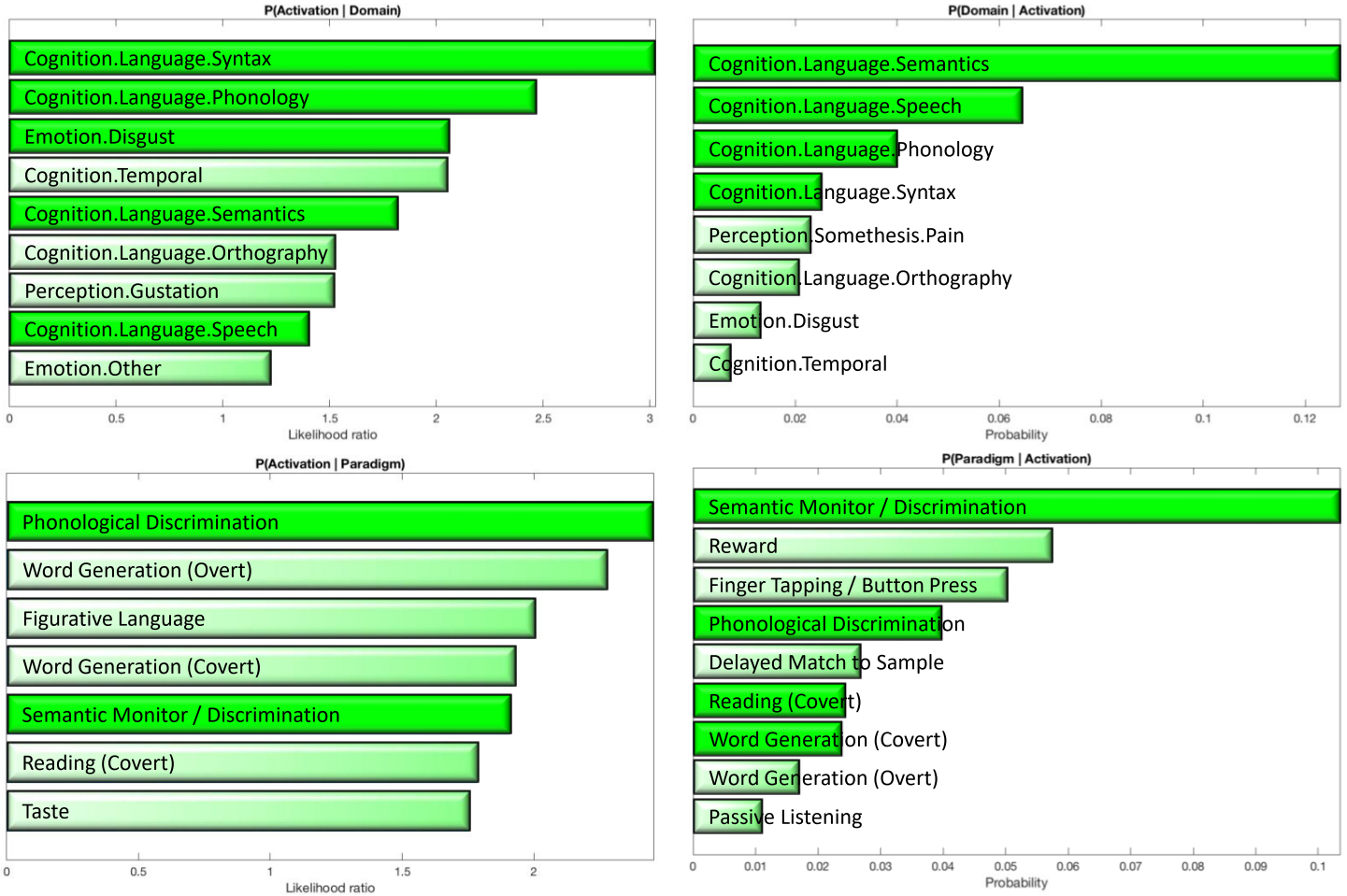

Fig. 20: Functional attribution of OP9 according to MACM analysis, regarding both hemispheres

Top row: most common BD; bottom row: most common PC; left column: likelihood ratio that activity in OP9 generates the BD/PC; right column: probability that the BD/PC will produce activation in OP9; full colour bars indicate remaining BD and PC after correction by FDR (false discovery rate).

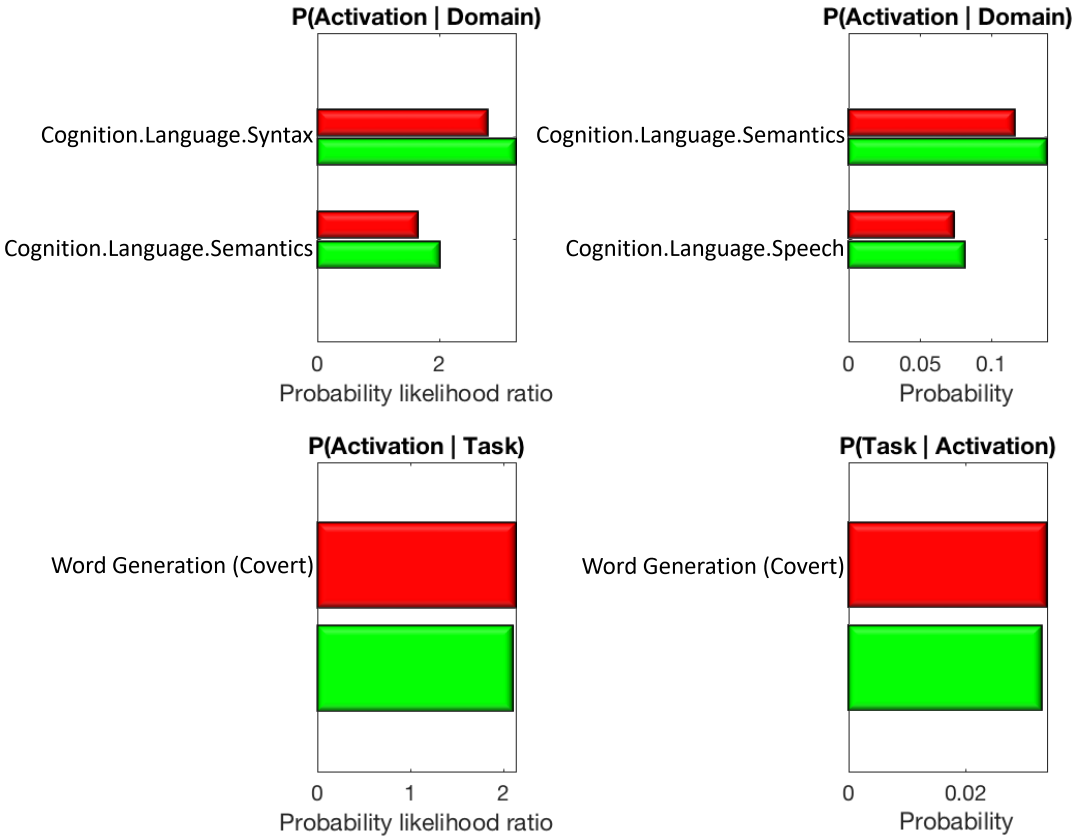

Fig. 21: Probability of activation of OP8 and OP9 by a given task according to forward inference of MACM analysis

Top row: most common BD; bottom row: most common PC; left column: likelihood ratio that activity in OP8 and OP9 generates the BD/PC; right column: probability that the BD/PC will produce activation in OP8 and OP9.

Activity in OP8 together with OP9 will produce language processing involving syntax, semantics or covert word generation more likely than other Behavioral Domains or Paradigm Classes. Similarly, activation is more likely observed in OP8 together with OP9, when similar Behavioral Domains – but speech instead of syntax – and Paradigm Classes are performed.

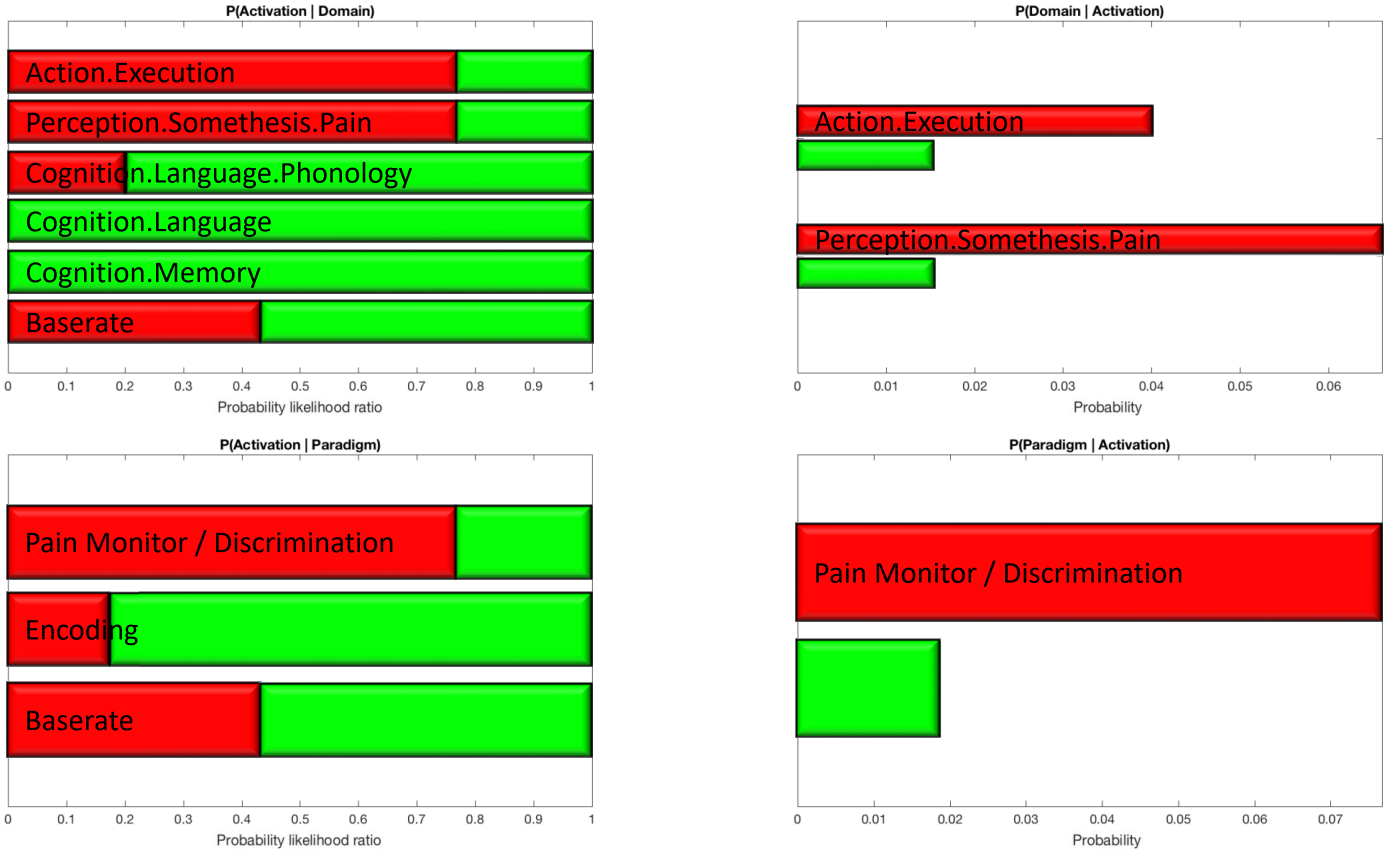

Fig. 22: Probability of inducing a task by activation of OP8 and OP9 according to reverse inference of MACM analysis

Top row: most common BD; bottom row: most common PC; left column: likelihood ratio that activity in OP8 and OP9 generates the BD/PC; right column: probability that the BD/PC will produce activation in OP8 and OP9.

OP8 rather induces action execution and pain perception and discrimination than OP9, while activation in OP9 more likely leads to language and memory operations. Note, that these last categories are only used, when the underlying experiments cannot be grouped in further subdomains.

The main PC for OP8 are covert word generation, thus a linguistic item, and pain discrimination and taste. Comparing the BDPC inter-hemispherically, language function is preliminarily executed by the left OP8, while the right one is more responsible for pain perception and discrimination. Taste is represented in both hemispheres.

OP9 is also involved in language processing regarding primarily syntax and semantics, but also phonology and speech. Like OP8, the PC also embrace covert word generation, additionally also overt word generation as well as phonological and semantic discrimination. Left OP9 is, alike left OP8, responsible for the language functions, whereas right OP9 is mainly responsible for the behavioural domain of pain perception and the temporal relation of events.

Areas OP8 and OP9 both participate in syntactic and semantic language processing, as well as covert word generation. In contrast to that, OP8 is more involved in action execution (other than speech) and pain perception, while OP9 is more involved in phonological and encoding tasks.

Analysis for co-activation showed comparable co-activations for OP8 and OP9 in both hemispheres (see **Figure 23**). As expected, activation is shown in the frontal operculum, representing both areas themselves. Further distinct activation could be found in the “classical Broca’s areas” (Broca, 1861) in the pars opercularis and triangularis of the inferior frontal gyrus, BA44 and BA45 (Amunts et al., 1999; Amunts et al., 2004). In small parts the co-activation reaches BA6 in the mid frontal gyrus (Geyer et al., 2004). In the parietal cortex, a small rostral part of the anterior parietal cortex representing BA1 (Geyer et al., 1999; Geyer et al., 2000) and of the inferior parietal cortex representing areas PF, PFt, PGa, PFm in the left hemisphere, respectively PGa and PFm in the right hemisphere (Caspers et al., 2006; Caspers et al., 2008) are co-activated. Especially in the left hemisphere of the superior temporal gyrus, co-activation can be found in regions represented by the caudal portions of area TE1.0, TE1.1 and TE1.2 (Morosan et al., 2001; Rademacher et al., 2001), forming BA41, and adjacent BA42. And finally co-activation can be observed in the caudal parts of the inferior temporal gyrus and partly fusiform gyrus,

represented mainly by BA37, as well as bihemispheric anterior lobe of the cerebellum.

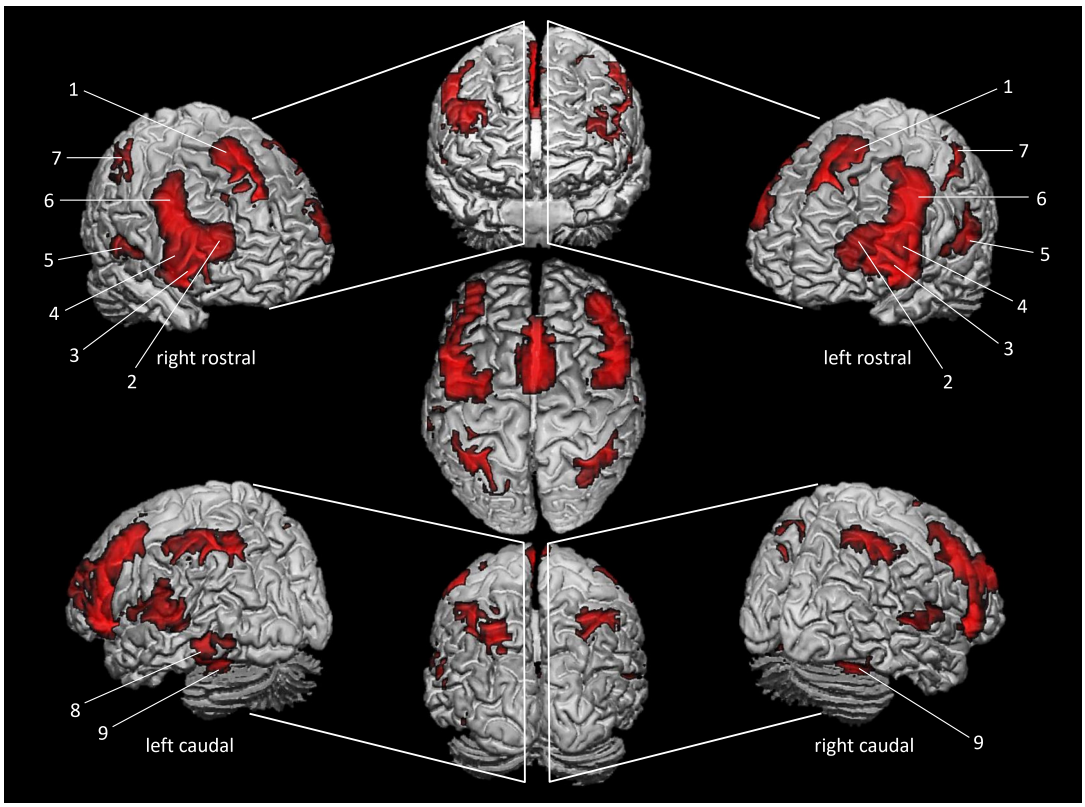

Fig. 23: 3D render of the co-activations of OP8 and OP9

Co-activations are shown as red areas, calculated by using meta-analytic connectivity modelling (MACM). Renderings in the middle column are shown from rostral (at the top), parietal (middle) and caudal (bottom), other views as depicted. Numbers decode the gyri at the specific location as follows:

1: gyrus frontalis superior; 2: gyrus frontalis medius; 3: gyrus frontalis inferior, pars triangularis; 4: gyrus frontalis inferior, pars opercularis; 5: gyrus temporalis superior; 6: gyrus praecentralis; 7: gyrus parietalis superior; 8: gyrus temporalis inferior; 9: lobus anterior cerebelli

Discussion

The observer-independent delineation of OP8 and OP9 reveals two new areas in the frontal operculum that have not been mapped before using a cytoarchitectonic approach. The present study depicts the laminar organization of OP8 and OP9. They are both dysgranular areas with a narrow, but distinctive lamina IV. Furthermore, there are few fairly prominent, mid-large pyramidal cells in lower lamina III and upper lamina V. Both areas could be verified in both hemispheres on the inside of the circular insular sulcus, without ever migrating over to the insular gyrus, and rarely reaching the lateral free cortical surface. Furthermore, we could prove their direct neighbourhood to “classical Broca’s areas” BA44 and BA45, as shown in a previous study based on receptor autoradiography (Amunts et al., 2010). Yet, their location, their hierarchical relations and their cortical symmetry contradict a strictly language related function.

Comparison with brain maps of Brodmann and Economo & Koskinas

Korbinian Brodmann used a light microscope and examined a single hemisphere of a single brain (Brodmann, 1909) to establish his famous map of cortical areas - nevertheless a revolutionary achievement in his period. In contrast to that, the main advantage of the now applied technique is the use of multiple probes and modern, observer-independent methods to reach statistical significance and universal validity. The methodical obstacles of the past may explain the obvious white spot that Brodmann left in his brain map in the depth of the lateral fissure. There is no sufficient description of areas in the depth of the sulci, especially in the depth of the lateral fissure and adjoining circular insular sulcus, in such necessary detail as now revealed. His BA43 is located on the Rolandic operculum at the ventral ending of the central sulcus. The rostral border is located at the anterior subcentral sulcus (BA6), the caudal and dorsal border is built by the posterior subcentral sulcus and the transition to BA40 (Area supramarginalis). This BA43 is described as extending on the inner side of the operculum and thus adjoining the insular cortex. The

cytoarchitecture of this area is “retrocentral”, thus containing a clear lamina IV and absent of giant pyramidal cells (Brodmann, 1909). The area rostral of BA43 and ventral of BA44 and BA45 is left undefined. According to our findings, the now delineated areas OP8 and OP9, located in the depth of the frontal operculum, ventromedial of BA44 and BA45, in their caudal extent match the rostral ending of BA43 and in their remaining dimension fill the non-described white spot, as his cytoarchitectonic characterization is comparable with our description of OP8 and OP9.

In the brain map of Economo and Koskinas (Economo and Koskinas, 1925), the equivalents of OP8 and OP9 are mainly located in the ventral parts of F*CD*op (Area frontalis intermedio granularis in operculo) and F*D*op (Area frontalis granularis in operculo), while they rostrally extend to F*F* (Area orbitalis) and caudally to F*B*op (Area frontalis agranularis in operculo). The microscopical description, especially of F*CD*op, by Economo and Koskinas correlates to our findings of OP8 and OP9, as they are described as slightly granular areas in transition from the adjacent agranular to more granular areas (Economo and Koskinas, 1925). Lamina III in those areas is described as broad and in its deep part packed with prominent large pyramidal cells, similar to upper lamina V. The latter one is then significantly lighter in its middle and deep parts. These descriptions match both areas OP8 and OP9 with slight, but distinguishable differences in cell density, distribution and dimension. Lamina IV is described to be interstratified with small pyramidal cells by Economo and Koskinas, which is also true for OP8 and OP9. Furthermore this lamina becomes better distinguishable in its more rostral location, thus matching our description of area OP9.

We can now provide advanced maps of areas OP8 and OP9 in the frontal operculum, which do not only enhance spatial details in terms of high resolution, but are also transferrable into the three dimensional room. Furthermore, they can be used as subject of further MACM analysis to reveal their role in brain processes and their co-activation with further brain regions.

Integration of cytoarchitectonic delineation into functional imaging analysis

As imaging modalities like fMRI and PET-CT are easily capable of illustrating the depth of sulci and define cortical characteristics, they still have a limitation in image resolution. Contrariwise, cytoarchitecture based areal delineation lacks information about distinctive areal function. Thus, these cytoarchitectonic maps can serve as the fundament of spatial and thus areal assignment of activation in fMRI or other functional imaging modalities. Our digitization resolution of 1.02 µm / pixel is about 100 times higher than that of a state of the art 11.75 Tesla MRI at about 100 µm / pixel. Thus, functional studies using current fMRI and PET-CT are inferior to further distinguish the cortical layers and provide the microstructural organization and areal subdivision of cortex in a proper quality comparable to light microscopy. There are many studies using these neuro-imaging techniques decoding the functional attribution of the FOP as a consortium of multiple areas, and thus potentially of therein enclosed areas OP8 and OP9. They attest primarily language related function, which was confirmed by our meta-analysis. As MACM can only serve as a vague indicator of areal functions, the following discussion of functional areal attribution is mostly done by reviewing single functional studies.

Connection of the FOP to other language related areas

The inferior frontal gyrus (IFG) can be subdivided into different subregions based on diffusion-based imaging and subsequent tractography by distinguishing cortical areas by their fibre-connections within the white matter (Anwander et al., 2007), including the FOP. Another subregion is built by BA44, as well as BA45 combined with BA47. These regions connect to different areas by a dorsal and a ventral pathway, resulting in several language related networks. The FOP is connected to the anterior superior temporal cortex via the uncinate fasciculus (Anwander et al., 2007; Friederici, Bahlmann et al., 2006; Hua et al., 2009; Thiebaut de Schotten et al., 2012). This part of the ventral pathway processes basic syntax, thus building a “ventral syntactic network” (Friederici and Chomsky, 2017). The more complex syntax is processed by a

“dorsal syntactic network” (Friederici and Chomsky, 2017) connecting BA44 of the inferior frontal gyrus with the posterior superior temporal cortex via the arcuate fasciculus and a minor part of the superior longitudinal fasciculus (Friederici, 2011) as a part of the dorsal pathway (Perani et al., 2011). For the sake of completeness, the other two parts of the ventral and dorsal pathway may be mentioned as well, as they differ in their functional attribution. The dorsal pathway connects the posterior temporal cortex via the superior longitudinal fasciculus and a minor part of the arcuate fasciculus with the premotor cortex in the inferior parietal lobe, as it is relevant for sensory-to-motor mapping and thus for repetition of someone’s speech (Saur et al., 2008). The ventral pathway connects BA45 and BA47 with the superior and middle temporal, as well as the occipital cortex, via the inferior fronto-occipital fasciculus, which equals the extreme capsule fibre system. This is relevant for semantic processing and thematic role assignment (Dapretto and Bookheimer, 1999; Friederici and Chomsky, 2017; Hagoort and Indefrey, 2014; Thompson-Schill et al., 1997).

Similar results have been proven by comparison of their receptor architecture. OP8 and OP9 showed much similarity in their receptor distribution pattern (Amunts et al., 2010). As postulated in other receptor autoradiography studies, areas with similar receptor distribution patterns process similar tasks (Zilles and Amunts, 2009; Zilles, Palomero-Gallagher et al., 2002). Hierarchical cluster analysis based on receptor analysis showed clusters of OP8 and OP9, which were different from another cluster, including BA44 and BA45 (Amunts et al., 2010). As the receptor fingerprints of the opercular areas differed from those of BA44 and BA45, we can correlate these differences with their diverging functionality. This is in line with the results of our current cytoarchitectonic hierarchical cluster analysis, which shows a grouping of OP8 and OP9 that can be distinguished from a clustering of BA44 and BA45 (see **Figure 15**). The hierarchical cluster analysis shows a greater similarity of OP8 and OP9 with BA47, which is part of the orbitofrontal areas. Yet, this cytoarchitectonic clustering differs from previously mentioned receptor architectonic clustering (Amunts et al., 2010), where the opercular areas build a higher-level cluster with BA44 and BA45 and show maximum distance to BA47. Comparing to functional

studies, these assign semantic functions to BA47 (Hagoort and Indefrey, 2014) in a controlling executive manner like word categorization (Thompson-Schill et al., 1997). This is a commonality with BA45, whereas BA44 showed to be more similar to the opercular areas as it rather participates in syntactic than semantic processes. Thus we can conclude that cytoarchitectonic similarity does not mandatory result in functional similarity.

The role of OP8 and OP9 in language processing

As shown by our MACM analysis, OP8 and OP9 are most notably involved in language processing. Integrating the cytoarchitectonically based exact location of both areas with activated foci in functional studies might lead to a more accurate functional attribution in the complex field of language.

The initial phrase structure building is based on syntax (Bornkessel and Schlesewsky, 2006; Friederici, 2002), as this allows a first fast partition of the given auditory information. The partitions are based on the limited amount of word category information (e.g. noun, verb, adjective, etc.), which allows to assume the structure of a phrase without regarding its semantic information. This is an automatic process (Hahne and Friederici, 2002). The involvement of the FOP in initial phrase structure building could be shown in a lesion study combined with ERP (event-related potentials), where the ELAN (early left anterior negativity) was missing in patients with left frontal lesions (Friederici et al., 1999). The ELAN usually appears at about 120 – 200ms as the second process after the initial acoustic processes and is thus at the basis of the core language system, which follows the processing order of phonology prior to syntax prior to semantics (Friederici and Chomsky, 2017). A further study showed the involvement of the FOP in processing of syntactic violations (Friederici et al., 2003). Here, the left posterior FOP is correlated as parts of BA6 and BA43, as well as parts of the insular cortex, and containing areas OP8 and OP9 (centres of activation at xyz -37,9,8 and 40,14,5 in Talairach & Tournoux space). In contrast to its adjacent opercular areas, left BA44 was not necessarily significantly activated by the specific tasks of that particular study. This may be due to its connection to language-related working memory rather

than basic on-line language processing (Friederici et al., 2003). This study also suggests, that the FOP is solely involved in syntactic violation processing, but not in that of semantic violations. Yet, there is no consent, if the ELAN represents the detection of syntactic errors in initial phrase structure building or the initial phrase structure building itself (Friederici and Chomsky, 2017).

Beyond involvement in initial phrase structure building, the FOP is described to be activated in the processing of transitional dependencies of sequences generated by finite state grammar (FSG) (Friederici, Bahlmann et al., 2006). The processing of FSG can be learned by non-human primates, which reflects that it is phylogenetically older cortex than BA44/45 (Amunts and Zilles, 2012), which are not involved in FSG. Breaking down to the most simple hierarchical syntactic phrase, the binding of two words - so called Merge (Chomsky, 2013) - the FOP is known to be an integral part of such processing accompanied by the anterior superior temporal gyrus (Zaccarella and Friederici, 2015). Yet, comparison of the described coordinates (xyz -36,16,0 in Talairach & Tournoux coordinates) suggests, that OP8 and OP9 are not necessarily involved in this process.

Furthermore, the FOP is also involved in the processing of phrase structure grammar (PSG) - here also evaluating aforementioned transitional dependencies. In contrast to FSG, the processing of PSG characterizes human language, there has been no evidence of learning compliance in non-human primates yet. Not only are BA44 and BA45 as phylogenetically younger cortex activated by the processing of complex hierarchical dependencies of sequences generated by PSG (Friederici, Bahlmann et al., 2006), but according to the coordinates described (xyz -46,16,8 in Talairach & Tournoux space), activation was also reported in both OP8 and OP9. The activation is independent of the difficulty of the hierarchical sequence, but of its presence in general (Friederici, Bahlmann et al., 2006).

Overall, the FOP seems to be part of a network with the anterior superior temporal gyrus for simple combinatory operations and with especially the ventral part of BA44 for local phrase structure building, thus leading regions for syntactic processing, while OP8 and OP9 as a small subregion of the FOP

together with BA44 are more involved in the processing of phrase structure grammar.

In contrast, BA45 is more involved in semantics. The similarity of the former areas is represented in their cytoarchitectonic structure. Frontal opercular areas OP8 and OP9, as well as BA44, are dysgranular areas with fairly prominent pyramidal cells in lower lamina III and upper lamina V and a narrow, but well visible lamina IV. The moderate lamination and visibility of columns is in common as well, albeit rudimentary in OP9. In contrast, the cytoarchitecture of BA45 is determined by its prominent and wider lamina IV, as well as a considerably bigger amount of large pyramidal cells especially in lamina III, and distinct lamination and visibility of columns. This suggests the assumption, that the comparable cytoarchitecture of OP8 and OP9 with BA44 is associated with their comparable function. The different cytoarchitecture of BA45 (and BA47) reflects their different function, as they process semantics and not syntax.

In ungrammatical violation of sentences, FOP has co-activations in the left postcentral gyrus, left cerebellum and right intraparietal sulcus (Friederici, Fiebach et al., 2006). In that study, areas OP8 (and probably dorsal border of OP9) were referred to as inferior portion of BA44 (xyz -49,10,4 in Talairach & Tournoux space). These findings correspond to our meta-analytic conjunctions for OP8 and OP9. Furthermore, we found quite equally distributed co-activation in the frontal inferior gyrus (BA 44, BA45, BA47), frontal superior gyrus (BA8), precentral gyrus (BA6), superior temporal gyrus (BA40-43), inferior temporal gyrus (BA21, BA37), as well as small parts of the cerebellum. The co-activation of BA8 might be as part of a circuit for working memory (Babiloni et al., 2005; Okuda et al., 2000; Rämä et al., 2001) and language processing (Carli et al., 2007). The same can be assumed for BA6 (Basho et al., 2007; Inui et al., 1998; Ranganath et al., 2003; Tulving et al., 1994). There is evidence for BA40 to participate in semantic processing, as well as auditory related working memory (Chou et al., 2006; Rämä et al., 2001). BA41 and BA42 are involved in auditory short-term memory (Zhang et al., 2003). Especially left hemispheric BA21 and BA37 take part in semantic processing (Chou et al., 2006; Düzel et al., 2001; McDermott et al., 2003) and word generation (Friedman et al., 1998). Functional studies describing language related processing of the FOP dependent on

sentence reading mainly report a focus of activation in the left hemisphere. Interestingly, this is not valid for grammatical processes related to auditory information.

Lateralization of function of OP8 and OP9

Regarding hemispherically dedicated functions, the right FOP is more activated by auditory stimulus than sentence reading as the left FOP (Friederici et al., 2000), as well as the processing of prosody / intonation (Meyer, M. et al., 2000). As Meyer et al. suggest, this might correspond to a scanning-process of sound for speech information (Meyer et al., 2002; Meyer et al., 2004; Meyer, E. et al., 2000). Processing of syntactic speech was reported in the rostral part of left OP9 (xyz -34,26,5 in Talairach and Tournoux space), while activation in right OP8 was induced by prosodic speech (xyz 43,10,8 and 43,12,9 in Talairach and Tournoux space). Yet, this only applies to pitch information without further lexical information. The involvement of lexical information in intonation, as in Mandarin Chinese, is also located in the left hemisphere (Gandour et al., 2004), as indicated by activation in bihemispherical OP9 (xyz -37,25,14 and 37,25,14 in Talairach and Tournoux space). Thus, despite the lack of significant cytoarchitectonic differences of both investigated areas, functional studies suggest a functional lateralization. A further hint to this discrepancy might be the slightly different receptor distribution pattern in both hemispheres in these areas, as shown for the M_2 receptor in a previous study (Amunts et al., 2010).

Functional interareal differentiation of OP8 and OP9

Compared to OP8, our BDPC of OP9 are even more focused on language function. As the PC show, activation in OP9 very likely results in overt and covert word generation, as well as phonological and semantic discrimination. This suggests a more active role of OP9 in language processing, while OP8 might be a more passive participator, for example in a controlling manner (see **Figure 19** and **Figure 20**). The confirmation of this thesis remains subject of further functional studies, as comparison with studies proving participation of

the FOP in task control as part of a network controlling cognitive processes shows differing results. In one study, OP8 and OP9 are not involved for the specific visual stimuli used in this study (house, body without head, face) (Higo et al., 2011). The centre of gravity in this study (xyz -30,22,-10 in Talairach and Tournoux space, xyz 34,18,-10 in MNI space respectively) focusses on an area in the same coronal, but more ventral plane, thus leaving our region of interest. Dosenbach et al. suggest the FOP, together with the anterior insular (aI) and dorsal anterior cingulate cortex (dACC) and medial superior frontal cortex (msFC), forming a core task-set system (Dosenbach et al., 2006). Both areas OP8 and OP9 might be involved, as the centre of gravity reported (xyz 35,17,5 in Talairach and Tournoux space) is exactly at the transition of the insula to the border of OP8 and OP9 in the maximum probability map. A recent study differed the FOP to be activated by performance monitoring, mostly together with the aI directly medially adjacent to OP8 and OP9 (Amiez et al., 2016).

Furthermore, a lesion-based study showed neighbouring defects in the left frontal opercular cortex in patients with apraxia of speech (Dronkers, 1996), with a peak described in the precentral gyrus in the insula (xyz -41,-2,10 in Talairach and Tournoux space). As this is right at the most dorsal ending of left OP8, this could lead to left OP8 being part of a network for planning articulatory movements.

Further evidence of lateralization of function beyond language processing

Morrison et al. found activation of supposedly left OP9 and right OP8 when subjects had to assess the interaction of object and action in a pain related fMRI study (appropriate: withdrawing hand from painful object / grabbing non-painful object vs. inappropriate: grabbing painful object / withdrawing hand from non-painful object) (Morrison et al., 2013). The cluster size is very small and the peak coordinates of activation (xyz -51,17,3 and 52,17,1 in MNI space) are very close to the border of OP8 and OP9 in both hemispheres, so no absolutely certain conclusion can be made, which of both areas is more involved. Unlike SII (OP1-4), this minor activation in OP8 and OP9 can hardly be taken as

significant evidence to count it part of a parietal sensorimotor circuit that SII is involved in. Probably OP8 and OP9 as part of the IFG participate in a network involving the superior parietal and frontal cortices, left posterior middle temporal cortex, midcingulate and cerebellum, which processes the assessment of object and action (Morrison et al., 2013, p. 1988). This seems to validate above mentioned role of the FOP in a core task-set system for performance monitoring (Dosenbach et al., 2006).

Nevertheless, regarding the results of our bihemispheric cytoarchitectonic mapping, that did not reveal significant left-right differences in the laminar structure of both areas, as well as the lack of a difference of volumes between both hemispheres, there is no distinct cytoarchitectonically justified clue of a lateralization. Contrariwise, adjacent BA44 and BA45 showed hemispherical differences in volume and receptor fingerprints (Amunts et al., 1999; Amunts et al., 2007; Amunts et al., 2010; Zilles et al., 2015).

Though being verified by reliable methods, there might be left minor uncertainties in above mentioned functional studies. There is certain evidence for a high interindividual variability of the borders of the FOP to the anterior insula in its entirety (Amiez et al., 2016; Naidich et al., 2004; Nieuwenhuys, 2012), as well as the assignment of activated voxels to their respective area due to cortical winding can be challenging and possibly misleading (Amiez et al., 2016). Furthermore, the resolution especially of MRI might be a limitation inherent of the method itself. Yet, as the cited functional analyses show similar results despite using different approaches, there seems to be significant evidence for the plausibility of the assumed functions of the FOP and OP8 and OP9 as its subregions.

Pain dependent activation of the FOP

Evidence has been provided that FOP is not exclusively involved in language tasks, but also other functions. In a recent study using nociceptive laser impulses while recording EEG via implanted EEG electrodes and thus high spatial resolution compared to regular EEG (Bastuji et al., 2016), the FOP is involved in the processing of nociceptive stimuli with an onset latency of about

134 ms. Yet, there is no clue of an involvement of areas OP8 and OP9 in these processes, as according to the mean MNI coordinates (xyz 46,3,11), the FOP observed in the study is slightly more posterior of our defined areas OP8 and OP9, thus possibly rather referring to the more caudodorsally located areas OP6-7 currently under observer-independent cytoarchitectonic mapping investigation.

Diseases effecting the FOP besides direct lesions

Besides direct lesions in the FOP, as forming the basis of above mentioned lesion based studies, there are only few diseases described yet, that specifically affect the frontal operculum, let alone OP8 and OP9 directly.

The progressive nonfluent aphasia (PNFA) is a frontotemporal lobar degeneration syndrome with mostly tau pathology attributed to atrophy of the left posterior frontal region – which in major meets well with OP8 and OP9 – as well as the left anterior insular region and basal ganglia (Ogar et al., 2007). It is characterized by certain speech deficits especially involving syntactic processing (apraxia of speech with consonant distortions, slow rate of speech and effortful articulation), as well as dysarthria (mostly hypernasality) in some cases. The PFNA is one of the very few non lesion based diseases that at least describes a direct involvement of the frontal operculum. As syntactic processing, that was shown to be a key role of OP8 and OP9 in brain function, is impaired in patients with PNFA, we can assume both areas to be directly affected. Yet, this thesis still remains to be proven.

Combining maps based on cytoarchitecture, receptor-autoradiography, tractography and functional imaging analysis could further help understanding the pathophysiology of similar diseases and help assigning functional deficits to their macro- and microstructural substrates.

Conclusion

For the first time, two frontal opercular areas OP8 and OP9 were identified and cytoarchitectonically mapped using an observer-independent approach. There has been no cytoarchitectonic correlate for the frontal operculum so far, despite a large number of functional studies that show activation in this brain region. Previous brain maps do not entirely describe areas in the depth of the sulci, or are only based on a small amount of investigated brains or only regarding one hemisphere. This was solved by delineation in both hemispheres of 10 brains.

The two new areas of the frontal operculum are closely related to the “classical Broca’s areas” BA44 and BA45; both are directly adjoining and they share several features of the laminar pattern. Their functional attribution to certain language processes, especially in the syntactic domain and basic local on-line phrase-structure building, has been proven in various functional studies. Yet, due to resolution deficits of these studies, the exact assignment of activation to specific areas within the frontal operculum has not been possible yet. With the cytoarchitectonic definition of the areas’ extent, this correlation can now be improved. As there is no method to provide structure and function, high definition spatial and temporal information, at the same time, the cytoarchitectonic delineation of OP8 and OP9 serves as base map with high resolution to further integrate with functional decoding. It will be publicly available as part of the probabilistic “Jubrain” brain atlas (Zilles and Amunts, 2010, online available at https://www.jubrain.fz-juelich.de/apps/cytoviewer/cytoviewer.php) and integrated into the “Human Brain Project” (online available at https://www.humanbrainproject.eu/en/).

The cytoarchitectonic mapping of the frontal operculum might also help improving other mapping modalities, like the Allen Brain Atlas (online available at portal.brain-map.org; Hawrylycz et al., 2012). This atlas of the human adult brain allows connecting genomic expression with brain anatomy based on MRI scans and diffusion tension imaging. Thus, by implementing cytoarchitectonically defined areal borders, the resolution and accuracy of specific areal gene expression might be improved for further correlation of genetic brain architecture and areal function.

Until now, neurolinguistic literature often uses superordinate anatomical labels, such as STG and FOP for describing the location of language processes and functional networks and connectivity. In contrast, due to former multimodal delineation, studies are much more precise in describing the “classical Broca‘s areas” BA44 and BA45, as well as BA47 (for example in Friederici and Chomsky, 2017). With now performed delineation of OP8 and OP9, as well as future cytoarchitectonic discrimination of further frontal opercular areas, the fundament is established for more fine-grained functional studies and more specific functional assignment. Furthermore, the cytoarchitectonic delineation of OP8 and OP9 raises the need to compare its characteristics to other areas known to be connected with the frontal operculum, especially regarding its linguistic functions, like the superior temporal gyrus.

As the FOP and thus OP8 and OP9 are potentially activated as part of a nociceptive processing circuit, further investigations of functional connectivity might reveal a link to the posterior parts of the parietal opercular areas OP1-4 forming the SII (Eickhoff, Schleicher et al., 2006), which is known to be involved in pain perception (Ferretti et al., 2003; Greenspan et al., 1999).

The refinement of brain mapping in the frontal operculum might also be helpful for clinical neurological and neurosurgical purpose. Not only can there be a more detailed discrimination of areas affected by stroke, cancer or other diseases. By integrating the new detailed maps in functional studies, more accurate forecast of the affected brain regions depending on the clinical functional deficits of a patient will be possible. Likewise, functional deficiencies due to neurosurgical interventions in the frontal operculum may be predicted more precisely and included in the planning of the procedure, thus helping in risk-benefit stratification.

References

Amiez, C., Wutte, M. G., Faillenot, I., Petrides, M., Burle, B. and Procyk, E. (2016) ‘Single subject analyses reveal consistent recruitment of frontal operculum in performance monitoring’, *NeuroImage*, vol. 133, pp. 266–278.

Amunts, K., Armstrong, E., Malikovic, A., Hömke, L., Mohlberg, H., Schleicher, A. and Zilles, K. (2007) ‘Gender-specific left-right asymmetries in human visual cortex’, *The Journal of neuroscience: the official journal of the Society for Neuroscience*, vol. 27, no. 6, pp. 1356–1364.

Amunts, K., Kedo, O., Kindler, M., Pieperhoff, P., Mohlberg, H., Shah, N. J., Habel, U., Schneider, F. and Zilles, K. (2005) ‘Cytoarchitectonic mapping of the human amygdala, hippocampal region and entorhinal cortex: Intersubject variability and probability maps’, *Anatomy and embryology*, vol. 210, 5-6, pp. 343–352.

Amunts, K., Lenzen, M., Friederici, A. D., Schleicher, A., Morosan, P., Palomero-Gallagher, N. and Zilles, K. (2010) ‘Broca's region: Novel organizational principles and multiple receptor mapping’, *PLoS biology*, vol. 8, no. 9.

Amunts, K., Malikovic, A., Mohlberg, H., Schormann, T. and Zilles, K. (2000) ‘Brodmann's areas 17 and 18 brought into stereotaxic space-where and how variable?’, *NeuroImage*, vol. 11, no. 1, pp. 66–84.

Amunts, K., Schleicher, A., Brgel, U., Mohlberg, H., Uylings, H. B. M. and Zilles, K. (1999) ‘Broca's region revisited: Cytoarchitecture and intersubject variability’, *The Journal of Comparative Neurology*, vol. 412, no. 2, pp. 319–341.

Amunts, K., Weiss, P. H., Mohlberg, H., Pieperhoff, P., Eickhoff, S. B., Gurd, J. M., Marshall, J. C., Shah, N. J., Fink, G. R. and Zilles, K. (2004) ‘Analysis of neural mechanisms underlying verbal fluency in cytoarchitectonically defined stereotaxic space--the roles of Brodmann areas 44 and 45’, *NeuroImage*, vol. 22, no. 1, pp. 42–56.

Amunts, K. and Zilles, K. (2001) ‘Advances in cytoarchitectonic mapping of the human cerebral cortex’, *Neuroimaging clinics of North America*, vol. 11, no. 2, 151-69, vii.

Amunts, K. and Zilles, K. (2012) ‘Architecture and organizational principles of Broca's region’, *Trends in Cognitive Sciences*, vol. 16, no. 8, pp. 418–426.

Amunts, K. and Zilles, K. (2015) ‘Architectonic Mapping of the Human Brain beyond Brodmann’, *Neuron*, vol. 88, no. 6, pp. 1086–1107.

Annett, M. (1973) ‘Handedness in families’, *Annals of human genetics*, vol. 37, no. 1, pp. 93–105.

Anwander, A., Tittgemeyer, M., Cramon, D. Y. von, Friederici, A. D. and Knosche, T. R. (2007) ‘Connectivity-Based Parcellation of Broca's Area’, *Cerebral cortex (New York, N.Y. : 1991)*, vol. 17, no. 4, pp. 816–825.

Babiloni, C., Ferretti, A., Del Gratta, C., Carducci, F., Vecchio, F., Romani, G. L. and Rossini, P. M. (2005) ‘Human cortical responses during one-bit delayed-response tasks: An fMRI study’, *Brain research bulletin*, vol. 65, no. 5, pp. 383–390.

Bailey, P. and Bonin, G. (1951) *The isocortex of man*, Urbana, University of Illinois Press.

Basho, S., Palmer, E. D., Rubio, M. A., Wulfeck, B. and Müller, R.-A. (2007) ‘Effects of generation mode in fMRI adaptations of semantic fluency: Paced production and overt speech’, *Neuropsychologia*, vol. 45, no. 8, pp. 1697–1706.

Bastuji, H., Frot, M., Perchet, C., Magnin, M. and Garcia-Larrea, L. (2016) 'Pain Networks From the Inside: Spatiotemporal Analysis of Brain Responses Leading From Nociception to Conscious Perception', *Human brain mapping*, vol. 47, pp. 4301–4315.

Bludau, S., Eickhoff, S. B., Mohlberg, H., Caspers, S., Laird, A. R., Fox, P. T., Schleicher, A., Zilles, K. and Amunts, K. (2014) 'Cytoarchitecture, probability maps and functions of the human frontal pole', *NeuroImage*, 93 Pt 2, pp. 260–275.

Bornkessel, I. and Schlesewsky, M. (2006) 'The extended argument dependency model: A neurocognitive approach to sentence comprehension across languages', *Psychological review*, vol. 113, no. 4, pp. 787–821.

Branch, C., Milner, B. and Rasmussen, T. (1964) 'Intracarotid sodium amytal for the lateralization of cerebral speech dominance: Observations in 123 Patients', *Journal of neurosurgery*, vol. 21, pp. 399–405.

Brett, M. (2009) *The MNI brain and the Talairach atlas* [Online], MRC Cognition and Brain Sciences Unit, University of Cambridge. Available at http://imaging.mrc-cbu.cam.ac.uk/imaging/MniTalairach (Accessed 12 October 2018).

Broca, P. (1861) 'Remarques sur le siège de la faculté du langage articulé, suivies d'une observation d'aphémie (perte de la parole)', *Bulletin et mémoires de la Société Anatomique de Paris*, vol. 6, pp. 330–357.

Brodmann, K. (1909) *Vergleichende Lokalisationslehre der Großhirnrinde in ihren Prinzipien dargestellt auf Grund des Zellenbaues.*, Leipzig, Barth.

Buxhoeveden, D. P., Switala, A. E., Roy, E. and Casanova, M. F. (2000) 'Quantitative analysis of cell columns in the cerebral cortex', *Journal of Neuroscience Methods*, vol. 97, no. 1, pp. 7–17.

Campbell, A. W. and Schlesinger, E. B. (1905) *Histological studies on the localisation of cerebral function*, Cambridge, University press.

Carli, D., Garreffa, G., Colonnese, C., Giulietti, G., Labruna, L., B., E., Ken, S., Macrì, M. A. and Maraviglia, B. (2007) 'Identification of activated regions during a language task', *Magnetic resonance imaging*, vol. 25, no. 6, pp. 933–938.

Caspers, S., Eickhoff, S. B., Geyer, S., Scheperjans, F., Mohlberg, H., Zilles, K. and Amunts, K. (2008) 'The human inferior parietal lobule in stereotaxic space', *Brain structure & function*, vol. 212, no. 6, pp. 481–495.

Caspers, S., Geyer, S., Schleicher, A., Mohlberg, H., Amunts, K. and Zilles, K. (2006) 'The human inferior parietal cortex: Cytoarchitectonic parcellation and interindividual variability', *NeuroImage*, vol. 33, no. 2, pp. 430–448.

Choi, H.-J., Zilles, K., Mohlberg, H., Schleicher, A., Fink, G. R., Armstrong, E. and Amunts, K. (2006) 'Cytoarchitectonic identification and probabilistic mapping of two distinct areas within the anterior ventral bank of the human intraparietal sulcus', *The Journal of comparative neurology*, vol. 495, no. 1, pp. 53–69.

Chomsky, N. (2013) 'Problems of projection', *Lingua*, vol. 130, pp. 33–49.

Chou, T.-L., Booth, J. R., Bitan, T., Burman, D. D., Bigio, J. D., Cone, N. E., Lu, D. and Cao, F. (2006) 'Developmental and skill effects on the neural correlates of semantic processing to visually presented words', *Human Brain Mapping*, vol. 27, no. 11, pp. 915–924.

Dapretto, M. and Bookheimer, S. Y. (1999) 'Form and content: Dissociating syntax and semantics in sentence comprehension', *Neuron*, vol. 24, no. 2, pp. 427–432.

Dixon, W. J., ed. (1988) *BMDP statistical software manual*, Berkeley, University of California Press.

Dosenbach, N. U. F., Visscher, K. M., Palmer, E. D., Miezin, F. M., Wenger, K. K., Kang, H. C., Burgund, E. D., Grimes, A. L., Schlaggar, B. L. and Petersen, S. E. (2006) 'A core system for the implementation of task sets', *Neuron*, vol. 50, no. 5, pp. 799–812.

Dronkers, N. F. (1996) 'A new brain region for coordinating speech articulation', *Nature*, vol. 384, pp. 159–161.

Duvernoy, H. M. and Bourgouin, P. (1999) *The human brain: Surface, three-dimensional sectional anatomy with MRI, and blood supply* [Online], 2nd edn, Wien, Springer. Available at http://www.loc.gov/catdir/enhancements/fy0812/99022443-d.html (Accessed 12 October 2018).

Düzel, E., Picton, T. W., Cabeza, R., Yonelinas, A. P., Scheich, H., Heinze, H. J. and Tulving, E. (2001) 'Comparative electrophysiological and hemodynamic measures of neural activation during memory-retrieval', *Human Brain Mapping*, vol. 13, no. 2, pp. 104–123.

Economo, K. von and Koskinas, G. N. (1925) *Die Cytoarchitektonik der Hirnrinde des erwachsenen Menschen.*, Wien, Springer.

Eickhoff, S. B., Amunts, K., Mohlberg, H. and Zilles, K. (2006) 'The human parietal operculum. II. Stereotaxic maps and correlation with functional imaging results', *Cerebral cortex (New York, N.Y. : 1991)*, vol. 16, no. 2, pp. 268–279.

Eickhoff, S. B., Bzdok, D., Laird, A. R., Kurth, F. and Fox, P. T. (2012) 'Activation likelihood estimation meta-analysis revisited', *NeuroImage*, vol. 59, no. 3, pp. 2349–2361.

Eickhoff, S. B., Heim, S., Zilles, K. and Amunts, K. (2006) 'Testing anatomically specified hypotheses in functional imaging using cytoarchitectonic maps', *NeuroImage*, vol. 32, no. 2, pp. 570–582.

Eickhoff, S. B., Jbabdi, S., Caspers, S., Laird, A. R., Fox, P. T., Zilles, K. and Behrens, T. E. J. (2010) 'Anatomical and functional connectivity of cytoarchitectonic areas within the human parietal operculum', *The Journal of neuroscience : the official journal of the Society for Neuroscience*, vol. 30, no. 18, pp. 6409–6421.

Eickhoff, S. B., Laird, A. R., Grefkes, C., W., L. E., Zilles, K. and Fox, P. T. (2009) 'Coordinate-based activation likelihood estimation meta-analysis of neuroimaging data: A random-effects approach based on empirical estimates of spatial uncertainty', *Human brain mapping*, vol. 30, no. 9, pp. 2907–2926.

Eickhoff, S. B., Schleicher, A., Zilles, K. and Amunts, K. (2006) 'The human parietal operculum. I. Cytoarchitectonic mapping of subdivisions', *Cerebral cortex (New York, N.Y. : 1991)*, vol. 16, no. 2, pp. 254–267.

Eickhoff, S. B., Stephan, K. E., Mohlberg, H., Grefkes, C., Fink, G. R., Amunts, K. and Zilles, K. (2005) 'A new SPM toolbox for combining probabilistic cytoarchitectonic maps and functional imaging data', *NeuroImage*, vol. 25, no. 4, pp. 1325–1335.

Evans, A. C., Collins, D. L., Janke, A. L. and Baillet, S. (2012) 'Brain templates and atlases', *NeuroImage*, vol. 62, no. 2, pp. 911–922.

Evans, A. C., Collins, D. L., Mills, S. R., Brown, E. D., Kelly, R. L. and Peters, T. M. (1994) *3D statistical neuroanatomical models from 305 MRI volumes*, New York, NY, Piscataway, NJ, Institute of Electrical and Electronics Engineers.

Evans, A. C., Marrett, S., Neelin, P., Collins, L., Worsley, K., Dai, W., Milot, S., Meyer, E. and Bub, D. (1992) 'Anatomical mapping of functional activation in stereotactic coordinate space', *NeuroImage*, vol. 1, no. 1, pp. 43–53.

Ferretti, A., Babiloni, C., Gratta, C. D., Caulo, M., Tartaro, A., Bonomo, L., Rossini, P. M. and Romani, G. L. (2003) 'Functional topography of the secondary somatosensory cortex for nonpainful and painful stimuli: An fMRI study', *NeuroImage*, vol. 20, no. 3, pp. 1625–1638.

Flechsig, P. E. (1920) *Anatomie des menschlichen Gehirns und Rückenmarks auf myelogenetischer Grundlage*, Leipzig, Thieme.

Fox, P. T., Laird, A. R., Fox, S. P., Fox, P. M., Uecker, A. M., Crank, M., Koenig, S. F. and Lancaster, J. L. (2005) 'BrainMap taxonomy of experimental design: Description and evaluation', *Human brain mapping*, vol. 25, no. 1, pp. 185–198.

Fox, P. T. and Lancaster, J. L. (2002) 'Opinion: Mapping context and content: the BrainMap model', *Nature reviews. Neuroscience*, vol. 3, no. 4, pp. 319–321 [Online]. DOI: 10.1038/nrn789.

Friederici, A. D. (2002) 'Towards a neural basis of auditory sentence processing', *Trends in Cognitive Sciences*, vol. 6, no. 2, pp. 78–84.

Friederici, A. D. (2011) 'The brain basis of language processing: from structure to function', *Physiological reviews*, vol. 91, no. 4, pp. 1357–1392.

Friederici, A. D., Bahlmann, J., Heim, S., Schubotz, R. I. and Anwander, A. (2006) 'The brain differentiates human and non-human grammars: functional localization and structural connectivity', *Proceedings of the National Academy of Sciences of the United States of America*, vol. 103, no. 7, pp. 2458–2463.

Friederici, A. D. and Chomsky, N. (2017) *Language in Our Brain: The Origins of a Uniquely Human Capacity*, Cambridge, MIT Press.

Friederici, A. D., Cramon, D. Y. von and Kotz, S. A. (1999) 'Language related brain potentials in patients with cortical and subcortical left hemisphere lesions', *Brain*, 122 (Pt 6), pp. 1033–1047.

Friederici, A. D., Fiebach, C. J., Schlesewsky, M., Bornkessel, I. D. and Cramon, D. Y. von (2006) 'Processing linguistic complexity and grammaticality in the left frontal cortex', *Cerebral cortex (New York, N.Y. : 1991)*, vol. 16, no. 12, pp. 1709–1717.

Friederici, A. D., Meyer, M. and Cramon, D. Y. von (2000) 'Auditory Language Comprehension: An Event-Related fMRI Study on the Processing of Syntactic and Lexical Information', *Brain and language*, vol. 74, pp. 289–300.

Friederici, A. D., Rüschemeyer, S.-A., Hahne, A. and Fiebach, C. J. (2003) 'The role of left inferior frontal and superior temporal cortex in sentence comprehension: Localizing syntactic and semantic processes', *Cerebral cortex (New York, N.Y. : 1991)*, vol. 13, no. 2, pp. 170–177.

Friedman, L., Kenny, J. T., Wise, A. L., Wu, D., Stuve, T. A., Miller, D. A., Jesberger, J. A. and Lewin, J. S. (1998) 'Brain activation during silent word generation evaluated with functional MRI', *Brain and language*, vol. 64, no. 2, pp. 231–256.

Gandour, J., Tong, Y., Wong, D., Talavage, T., Dzemidzic, M., Xu, Y., Li, X. and Lowe, M. (2004) 'Hemispheric roles in the perception of speech prosody', *NeuroImage*, vol. 23, no. 1, pp. 344–357.

Geyer, S., Christ, B., Kriz, W., Kummer, W., Marani, E., Putz, R., Sano, Y., Schiebler, T. H. and Zilles, K. (2004) *The Microstructural Border Between the Motor and the Cognitive Domain in the Human Cerebral Cortex: With 3 tables*, Berlin, Heidelberg, Springer Berlin Heidelberg.

Geyer, S., Schleicher, A. and Zilles, K. (1999) 'Areas 3a, 3b, and 1 of human primary somatosensory cortex', *NeuroImage*, vol. 10, no. 1, pp. 63–83.

Geyer, S., Schormann, T., Mohlberg, H. and Zilles, K. (2000) 'Areas 3a, 3b, and 1 of human primary somatosensory cortex. Part 2. Spatial normalization to standard anatomical space', *NeuroImage*, vol. 11, 6 Pt 1, pp. 684–696.

Greenspan, J. D., Lee, R. R. and Lenz, F. A. (1999) 'Pain sensitivity alterations as a function of lesion location in the parasylvian cortex', *Pain*, vol. 81, no. 3, pp. 273–282.

Hagoort, P. (2005) 'On Broca, brain, and binding: a new framework', *Trends in Cognitive Sciences*, vol. 9, no. 9, pp. 416–423.

Hagoort, P. and Indefrey, P. (2014) 'The neurobiology of language beyond single words', *Annual review of neuroscience*, vol. 37, pp. 347–362.

Hahne, A. and Friederici, A. D. (2002) 'Differential task effects on semantic and syntactic processes as revealed by ERPs', *Cognitive Brain Research*, vol. 13, no. 3, pp. 339–356.

Hawrylycz, M. J., Lein, E. S., Guillozet-Bongaarts, A. L., Shen, E. H., Ng, L., Miller, J. A., van de Lagemaat, L. N., Smith, K. A., Ebbert, A., Riley, Z. L., Abajian, C., Beckmann, C. F., Bernard, A., Bertagnolli, D., Boe, A. F., Cartagena, P. M., Chakravarty, M. M., Chapin, M., Chong, J., Dalley, R. A., David Daly, B., Dang, C., Datta, S., Dee, N., Dolbeare, T. A., Faber, V., Feng, D., Fowler, D. R., Goldy, J., Gregor, B. W., Haradon, Z., Haynor, D. R., Hohmann, J. G., Horvath, S., Howard, R. E., Jeromin, A., Jochim, J. M., Kinnunen, M., Lau, C., Lazarz, E. T., Lee, C., Lemon, T. A., Li, L., Li, Y., Morris, J. A., Overly, C. C., Parker, P. D., Parry, S. E., Reding, M., Royall, J. J., Schulkin, J., Sequeira, P. A., Slaughterbeck, C. R., Smith, S. C., Sodt, A. J., Sunkin, S. M., Swanson, B. E., Vawter, M. P., Williams, D., Wohnoutka, P., Zielke, H. R., Geschwind, D. H., Hof, P. R., Smith, S. M., Koch, C., Grant, S. G. N. and Jones, A. R. (2012) 'An anatomically comprehensive atlas of the adult human brain transcriptome', *Nature*, vol. 489, no. 7416, pp. 391–399.

Henn, S., Schormann, T., Engler, K., Zilles, K. and Witsch, K. (1997) *Elastische Anpassung in der digitlaen Bildverarbeitung auf mehreren Auflösungsstufen mit Hilfe von Mehrgitterverfahren*, Berlin, Heidelberg, Springer.

Henssen, A., Zilles, K., Palomero-Gallagher, N., Schleicher, A., Mohlberg, H., Gerboga, F., Eickhoff, S. B., Bludau, S. and Amunts, K. (2016) 'Cytoarchitecture and probability maps of the human medial orbitofrontal cortex', *Cortex*, vol. 75, pp. 87–112.

Higo, T., Mars, R. B., Boorman, E. D., Buch, E. R. and Rushworth, M. F. S. (2011) 'Distributed and causal influence of frontal operculum in task control', *Proceedings of the National Academy of Sciences of the United States of America*, vol. 108, no. 10, pp. 4230–4235.

Hömke, L. (2006) ‘A multigrid method for anisotropic PDEs in elastic image registration’, *Numerical Linear Algebra with Applications*, vol. 13, 2-3, pp. 215–229.

Howard, C. V. and Reed, M. G. (1998) *Unbiased stereology: Three-dimensional measurement in microscopy*, Oxford, BIOS Scientific Publ.

Hua, K., Oishi, K., Zhang, J., Wakana, S., Yoshioka, T., Zhang, W., Akhter, K. D., Li, X., Huang, H., Jiang, H., van Zijl, P. and Mori, S. (2009) ‘Mapping of functional areas in the human cortex based on connectivity through association fibers’, *Cerebral cortex (New York, N.Y. : 1991)*, vol. 19, no. 8, pp. 1889–1895.

Inui, T., Otsu, Y., Tanaka, S., Okada, T., Nishizawa, S. and Konishi, J. (1998) ‘A functional MRI analysis of comprehension processes of Japanese sentences’, *Neuroreport*, vol. 9, no. 14, pp. 3325–3328.

Jones, S. E., Buchbinder, B. R. and Aharon, I. (2000) ‘Three-dimensional mapping of cortical thickness using Laplace's Equation’, *Human Brain Mapping*, vol. 11, no. 1, pp. 12–32.

Just, M. A., Carpenter, P. A., Keller, T. A., Eddy, W. F. and Thulborn, K. R. (1994) ‘Brain Activation Modulated by Sentence Comprehension’, *Science*, no. 274, pp. 114–116.

Laird, A. R., Eickhoff, S. B., Li, K., Robin, D. A., Glahn, D. C. and Fox, P. T. (2009) ‘Investigating the functional heterogeneity of the default mode network using coordinate-based meta-analytic modeling’, *The Journal of neuroscience : the official journal of the Society for Neuroscience*, vol. 29, no. 46, pp. 14496–14505.

Laird, A. R., Fox, P. M., Price, C. J., Glahn, D. C., Uecker, A. M., Lancaster, J. L., Turkeltaub, P. E., Kochunov, P. and Fox, P. T. (2005) ‘ALE meta-analysis: Controlling the false discovery rate and performing statistical contrasts’, *Human brain mapping*, vol. 25, no. 1, pp. 155–164.

Mahalanobis, P. C., Majumda, D. N. and Rao, C. R. (1949) *Anthropometric survey of the united provinces.: A statistical study.*, Sankhya.

McDermott, K. B., Petersen, S. E., Watson, J. M. and Ojemann, J. G. (2003) ‘A procedure for identifying regions preferentially activated by attention to semantic and phonological relations using functional magnetic resonance imaging’, *Neuropsychologia*, vol. 41, no. 3, pp. 293–303.

Merker, B. (1983) ‘Silver staining of cell bodies by means of physical development’, *Journal of Neuroscience Methods*, vol. 9, no. 3, pp. 235–241.

Meyer, E., Friederici, A. D. and Cramon, D. Y. von (2000) ‘Neurocognition of auditory sentence comprehension: Event related fMRI reveals sensitivity to syntactic violations and task demands’, *Cognitive Brain Research*, vol. 9, no. 1, pp. 19–33.

Meyer, M., Alter, K., Friederici, A. D. and Cramon, D. Y. von (2000) ‘Different hemodynamic responses to sentence-level syntactic and prosodic processing’, *NeuroImage*, vol. 11, no. 5, p. 281.

Meyer, M., Alter, K., Friederici, A. D., Lohmann, G. and Cramon, D. Y. von (2002) ‘FMRI reveals brain regions mediating slow prosodic modulations in spoken sentences’, *Human brain mapping*, vol. 17, no. 2, pp. 73–88.

Meyer, M., Steinhauer, K., Alter, K., Friederici, A. D. and Cramon, D.Y. von (2004) ‘Brain activity varies with modulation of dynamic pitch variance in sentence melody’, *Brain and language*, vol. 89, no. 2, pp. 277–289.

Mohlberg, H., Lerch, J., Amunts, K., Evans, A. C. and Zilles, K. (2003) ‘Probabilistic cytoarchitectonic maps transformed into MNI space’, Poster number: 905, *NeuroImage*, vol. 19, no. 2, pp. 1763–1764.

Morosan, P., Rademacher, J., Schleicher, A., Amunts, K., Schormann, T. and Zilles, K. (2001) ‘Human primary auditory cortex: Cytoarchitectonic subdivisions and mapping into a spatial reference system’, *NeuroImage*, vol. 13, no. 4, pp. 684–701.

Morrison, I., Tipper, S. P., Fenton-Adams, W. L. and Bach, P. (2013) ‘"Feeling" others' painful actions: The sensorimotor integration of pain and action information’, *Human brain mapping*, vol. 34, no. 8, pp. 1982–1998.

Naidich, T. P., Kang, E., Fatterpekar, G. M., Delman, B. N., Gultekin, S. H., Wolfe, D., Ortiz, O., Yousry, I., Weismann, M. and Yousry, T. A. (2004) ‘The insula: Anatomic study and MR imaging display at 1.5 T’, *AJNR. American journal of neuroradiology*, vol. 25, no. 2, pp. 222–232.

Nieuwenhuys, R. (2012) ‘The insular cortex: A review’, *Progress in brain research*, vol. 195, pp. 123–163.

Ogar, J. M., Dronkers, N. F., Brambati, S. M., Miller, B. L. and Gorno-Tempini, M. L. (2007) ‘Progressive nonfluent aphasia and its characteristic motor speech deficits’, *Alzheimer disease and associated disorders*, vol. 21, no. 4, S23-30.

Okuda, J., Fujii, T., Yamadori, A., Kawashima, R., Tsukiura, T., Ohtake, H., Fukatsu, R., Suzuki, K., Itoh, M. and Fukuda, H. (2000) ‘Retention of words in long-term memory: A functional neuroanatomical study with PET’, *Neuroreport*, vol. 11, no. 2, pp. 323–328.

Ongür, D., Ferry, A. T. and Price, J. L. (2003) ‘Architectonic subdivision of the human orbital and medial prefrontal cortex’, *The Journal of comparative neurology*, vol. 460, no. 3, pp. 425–449.

Ono, M., Kubik, S., Abernathey, C. D. and Yaşargil, M. G. (1990) *Atlas of the cerebral sulci*, Stuttgart, Georg Thieme Verlag.

Perani, D., Saccuman, M. C., Scifo, P., Anwander, A., Awander, A., Spada, D., Baldoli, C., Poloniato, A., Lohmann, G. and Friederici, A. D. (2011) ‘Neural language networks at birth’, *Proceedings of the National Academy of Sciences of the United States of America*, vol. 108, no. 38, pp. 16056–16061.

Petrides, M. and Pandya, D. N. (2012) ‘The Frontal Cortex: Second Edition’, pp. 988–1011.

Rademacher, J., Morosan, P., Schormann, T., Schleicher, A., Werner, C., Freund, H. J. and Zilles, K. (2001) ‘Probabilistic mapping and volume measurement of human primary auditory cortex’, *NeuroImage*, vol. 13, no. 4, pp. 669–683.

Rämä, P., Martinkauppi, S., Linnankoski, I., Koivisto, J., Aronen, H. J. and Carlson, S. (2001) ‘Working memory of identification of emotional vocal expressions: An fMRI study’, *NeuroImage*, vol. 13, 6 Pt 1, pp. 1090–1101.

Ranganath, C., Johnson, M. K. and D'Esposito, M. (2003) ‘Prefrontal activity associated with working memory and episodic long-term memory’, *Neuropsychologia*, vol. 41, no. 3, pp. 378–389.

Riès, S. K., Xie, K., Haaland, K. Y., Dronkers, N. F. and Knight, R. T. (2013) ‘Role of the lateral prefrontal cortex in speech monitoring’, *Frontiers in human neuroscience*, vol. 7, pp. 1–16.

Roland, P. E., Geyer, S., Amunts, K., Schormann, T., Schleicher, A., Malikovic, A. and Zilles, K. (1997) ‘Cytoarchitectural maps of the human brain in standard anatomical space’, *Human Brain Mapping*, vol. 5, no. 4, pp. 222–227.

Rolston, J. D., Englot, D. J., Benet, A., Li, J., Cha, S. and Berger, M. S. (2015) ‘Frontal operculum gliomas: Language outcome following resection’, *Journal of neurosurgery*, vol. 122, no. 4, pp. 725–734.

Sanides, F. (1962) *Die Architektonik des Menschlichen Stirnhirns: Zugleich eine Darstellung der Prinzipien Seiner Gestaltung als Spiegel der Stammesgeschichtlichen Differenzierung der Grosshirnrinde*, Berlin, Heidelberg, s.l., Springer Berlin Heidelberg.

Sarkisov, S. A., Filimonoff, I. N. and Preobrashenskaya, N. S. (1949) *Cytoarchitecture of the human cortex cerebri (rus)*, Moscow, Medgiz.

Saur, D., Kreher, B. W., Schnell, S., Kümmerer, D., Kellmeyer, P., Vry, M.-S., Umarova, R., Musso, M., Glauche, V., Abel, S., Huber, W., Rijntjes, M., Hennig, J. and Weiller, C. (2008) ‘Ventral and dorsal pathways for language’, *Proceedings of the National Academy of Sciences of the United States of America*, vol. 105, no. 46, pp. 18035–18040.

Schleicher, A., Amunts, K., Geyer, S., Kowalski, T., Schormann, T., Palomero-Gallagher, N. and Zilles, K. (2000) ‘A stereological approach to human cortical architecture: Identification and delineation of cortical areas’, *Journal of Chemical Neuroanatomy*, vol. 20, no. 1, pp. 31–47.

Schleicher, A., Amunts, K., Geyer, S., Morosan, P. and Zilles, K. (1999) ‘Observer-independent method for microstructural parcellation of cerebral cortex: A quantitative approach to cytoarchitectonics’, *NeuroImage*, vol. 9, no. 1, pp. 165–177.

Schleicher, A., Morosan, P., Amunts, K. and Zilles, K. (2009) ‘Quantitative architectural analysis: A new approach to cortical mapping’, *Journal of autism and developmental disorders*, vol. 39, no. 11, pp. 1568–1581.

Schleicher, A., Palomero-Gallagher, N., Morosan, P., Eickhoff, S. B., Kowalski, T., Vos, K. de, Amunts, K. and Zilles, K. (2005) ‘Quantitative architectural analysis: A new approach to cortical mapping’, *Anatomy and embryology*, vol. 210, 5-6, pp. 373–386.

Schleicher, A. and Zilles, K. (1990) ‘A quantitative approach to cytoarchitectonics: Analysis of structural inhomogeneities in nervous tissue using an image analyser’, *Journal of Microscopy*, vol. 157, no. 3, pp. 367–381.

Stromswold, K., Caplan, D., Alpert, N. and Rauch, S. (1996) ‘Localization of syntactic comprehension by positron emission tomography’, *Brain and language*, vol. 52, no. 3, pp. 452–473.

Talairach, J., Tournoux, P. and Rayport, M. (1997) *Co-planar stereotaxic atlas of the human brain: 3-dimensional proportional system: an approach to cerebral imaging*, Stuttgart, Thieme.

Thiebaut de Schotten, M., Dell'Acqua, F., Valabregue, R. and Catani, M. (2012) ‘Monkey to human comparative anatomy of the frontal lobe association tracts’, *Cortex; a journal devoted to the study of the nervous system and behavior*, vol. 48, no. 1, pp. 82–96.

Thompson-Schill, S. L., D'Esposito, M., Aguirre, G. K. and Farah, M. J. (1997) ‘Role of left inferior prefrontal cortex in retrieval of semantic knowledge: A reevaluation’, *Proceedings of the National Academy of Sciences*, vol. 94, no. 26, pp. 14792–14797.

Tulving, E., Kapur, S., Markowitsch, H. J., Craik, F. I., Habib, R. and Houle, S. (1994) 'Neuroanatomical correlates of retrieval in episodic memory: Auditory sentence recognition', *Proceedings of the National Academy of Sciences of the United States of America*, vol. 91, no. 6, pp. 2012–2015.

Turkeltaub, P. E., Eden, G. F., Jones, K. M. and Zeffiro, T. A. (2002) 'Meta-Analysis of the Functional Neuroanatomy of Single-Word Reading: Method and Validation', *NeuroImage*, vol. 16, no. 3, pp. 765–780.

Tzourio-Mazoyer, N., Landeau, B., Papathanassiou, D., Crivello, F., Etard, O., Delcroix, N., Mazoyer, B. and Joliot, M. (2002) 'Automated anatomical labeling of activations in SPM using a macroscopic anatomical parcellation of the MNI MRI single-subject brain', *NeuroImage*, vol. 15, no. 1, pp. 273–289.

Ullman, M. T. (2001) 'A neurocognitiv perspective on language // A neurocognitive perspective on language: the declarative procedural model // The declarative/procedural model', *Nature Reviews Neuroscience*, vol. 2, no. 10, pp. 717–726.

Ullman, M. T., Corkin, S., Coppola, M., Hickok, G., Growdon, J. H., Koroshetz, W. J. and Pinker, S. (1997) 'A Neural Dissociation within Language: Evidence that the Mental Dictionary Is Part of Declarative Memory, and that Grammatical Rules Are Processed by the Procedural System', *Journal of cognitive neuroscience*, vol. 9, no. 2, pp. 266–276.

Uylings, H. B., Zilles, K. and Rajkowska, G. (1999) 'Optimal staining methods for delineation of cortical areas and neuron counts in human brains', *NeuroImage*, vol. 9, no. 4, pp. 439–445.

Uylings, H.B.M., van Eden, C. G. and Hofman, M. A. (1986) 'Morphometry of size/volume variables and comparison of their bivariate relations in the nervous system under different conditions', *Journal of Neuroscience Methods*, vol. 18, 1-2, pp. 19–37.

Vogt, C. and Vogt, O. (1919) 'Allgemeinere Ergebnisse unserer Hirnforschung', *Journal für Psychologie und Neurologie ; 25,Erg.h.1. S. 278 - 462*.

Ward jr., J. H. (1963) 'Hierarchical grouping to optimize an objective function', *Journal of the American Statistical Association : JASA*, 58 (1963), pp. 236–244.

Wree, A., Schleicher, A. and Zilles, K. (1982) 'Estimation of volume fractions in nervous tissue with an image analyzer', *Journal of Neuroscience Methods*, vol. 6, 1-2, pp. 29–43.

Zaccarella, E. and Friederici, A. D. (2015) 'Merge in the Human Brain: A Sub-Region Based Functional Investigation in the Left Pars Opercularis', *Frontiers in psychology*, vol. 6, p. 1818.

Zhang, D. R., Li, Z. H., Chen, X. C., Wang, Z. X., Zhang, X. C., Meng, X. M., He, S. and Hu, X. P. (2003) 'Functional comparison of primacy, middle and recency retrieval in human auditory short-term memory: An event-related fMRI study', *Cognitive Brain Research*, vol. 16, no. 1, pp. 91–98.

Zilles, K. and Amunts, K. (2009) 'Receptor mapping: Architecture of the human cerebral cortex', *Current opinion in neurology*, vol. 22, no. 4, pp. 331–339.

Zilles, K. and Amunts, K. (2010) 'Centenary of Brodmann's map--conception and fate', *Nature reviews. Neuroscience*, vol. 11, no. 2, pp. 139–145.

Zilles, K. and Amunts, K. (2013) ‘Individual variability is not noise’, *Trends in Cognitive Sciences*, vol. 17, no. 4, pp. 153–155.

Zilles, K., Armstrong, E., Schleicher, A. and Kretschmann, H.-J. (1988) ‘The human pattern of gyrification in the cerebral cortex’, *Anatomy and Embryology*, vol. 179, no. 2, pp. 173–179.

Zilles, K., Bacha-Trams, M., Palomero-Gallagher, N., Amunts, K. and Friederici, A. D. (2015) ‘Common molecular basis of the sentence comprehension network revealed by neurotransmitter receptor fingerprints’, *Cortex*, vol. 63, pp. 79–89.

Zilles, K., Palomero-Gallagher, N., Grefkes, C., Scheperjans, F., Boy, C., Amunts, K. and Schleicher, A. (2002) ‘Architectonics of the human cerebral cortex and transmitter receptor fingerprints: Reconciling functional neuroanatomy and neurochemistry’, *European neuropsychopharmacology : the journal of the European College of Neuropsychopharmacology*, vol. 12, no. 6, pp. 587–599.

Zilles, K., Schleicher, A., Palomero-Gallagher, N. and Amunts, K. (2002) ‘Quantitative Analysis of Cyto- and Receptor Architecture of the Human Brain’, in *Brain Mapping: The Methods,* Elsevier, pp. 573–602.

Danksagung

Größter Dank gilt Frau Prof. Dr. K. Amunts für die Vergabe und Betreuung meines Dissertationsvorhabens, sowie für ihre schier unermessliche Geduld, Unterstützung und ein stets offenes Ohr für Fragen und Vorschläge.

Für den wesentlichen Anstoß und die Ermöglichung, dieses Projekt durchzuführen, danke ich Herrn Prof. Dr. K. Zilles.

Herrn Prof. Dr. S. Eickhoff danke ich für die Beratung und Unterstützung bei der Metaanalyse.

Weiterer Dank gilt Herrn Dr. S. Bludau und Herrn. Dr. H. Mohlberg für die stete enge Betreuung bei der Methodik und Vorschlägen und Hilfestellungen in allen Bereichen dieser Arbeit.

Herrn R. Hübbers danke ich für die Unterstützung bei Hard- und Softwareproblemen, sowie dem ein oder anderen Transport von Gehirnschnitten zwischen Düsseldorf und Jülich.

Frau Dr. S. Bradler danke ich für Ihre Beratung und Unterstützung bei der Mikroskopie von hunderten Gehirnschnitten.

Ich danke Frau N. Unger und Frau F. Iannilli für die gemeinsame Differenzierung und Zuordnung der benachbarten operkularen Areale.

Für die Einführung in die Methodik und die Betreuung bei deren Anwendung danke ich Herrn Dr. A. Schleicher.

Für das immer zeitgerechte Heraussuchen der benötigten Materialen aus den Hirnarchiven im Forschungszentrum Jülich und im C&O Vogt Institut für Hirnforschung der Universität Düsseldorf bedanke ich mich bei Frau F. Kocaer und Herrn U. Opfermann.

Zu guter Letzt gilt mein persönlicher Dank meiner Familie und meiner Frau Maria für ihre Förderungen, Verständnis und Glauben an mich.